

# Strong pinning theory of thermal vortex creep in type II superconductors

M. Buchacek,<sup>1</sup> R. Willa,<sup>2</sup> V.B. Geshkenbein,<sup>1</sup> and G. Blatter<sup>1</sup>

<sup>1</sup>*Institute for Theoretical Physics, ETH Zurich, 8093 Zurich Switzerland*

<sup>2</sup>*Materials Science Division, Argonne National Laboratory, Lemont, IL 60439, USA*

(Dated: March 17, 2022)

We study thermal effects on pinning and creep in type-II superconductors where vortices interact with a low density  $n_p$  of strong point-like defects with pinning energy  $e_p$  and extension  $\xi$ , the vortex core size. Defects are classified as strong if the interaction between a single pin and an individual vortex leads to the appearance of bistable solutions describing pinned and free vortex configurations. Extending the strong pinning theory to account for thermal fluctuations, we provide a quantitative analysis of vortex depinning and creep. We determine the thermally activated transitions between bistable states using Kramer's rate theory and find the non-equilibrium steady-state occupation of vortex states. The latter depends on the temperature  $T$  and vortex velocity  $v$  and determines the current–voltage (or force–velocity) characteristic of the superconductor at finite temperatures. We find that the  $T = 0$  linear excess-current characteristic  $v \propto (j - j_c) \Theta(j - j_c)$  with its sharp transition at the critical current density  $j_c$ , keeps its overall shape but is modified in three ways due to thermal creep: a downward renormalization of  $j_c$  to the thermal depinning current density  $j_{dp}(T) < j_c$ , a smooth rounding of the characteristic around  $j_{dp}(T)$ , and the appearance of thermally assisted flux flow (TAFF)  $v \propto j \exp(-U_0/k_B T)$  at small drive  $j \ll j_c$ , with the activation barrier  $U_0$  defined through the energy landscape at the intersection of free and pinned branches. This characteristic emphasizes the persistence of pinning of creep at current densities beyond critical.

## I. INTRODUCTION

The properties of numerous materials are determined by the presence of topological excitations in the ordered states of matter; examples include vortices in type-II superconductors<sup>1,2</sup>, domain walls in ferroic materials<sup>3,4</sup>, or dislocations in metals<sup>5,6</sup>. The motion of such objects within the host material has a significant effect on its response, e.g., the onset of finite resistivity in superconductors or the loss of coercivity in magnets. Immobilizing these excitations, usually by pinning onto material defects, is thus of great technological relevance. The dynamics of topological objects then exhibits a transition between a static or pinned phase and a sliding or unpinned phase upon exceeding a threshold or critical force  $F_c$ . Understanding the pinned-to-sliding transition, optimizing the pinning threshold, and stabilizing it against thermal fluctuations present vital tasks at the cross-roads of disordered statistical physics and non-equilibrium phenomena. The complete description of the material's response is captured by the force–velocity ( $F - v$ ) characteristic of topological excitations; here, we extend the strong pinning theory to include effects of finite temperatures and calculate the response characteristic of vortex matter in type-II superconductors subject to a low density of point-like strong defects.

Vortex pinning is described by either of two frameworks: within weak pinning theory<sup>1,7</sup>, the pinning force due to an individual defect vanishes and it is the collective action of many defects which generates the average pinning-force density. On the contrary, for strong pinning<sup>7,8</sup>, individual defects induce substantial deformations that lead to bistable behavior and generate an average non-zero pinning force on the vortex lattice that scales linearly in the (small) density  $n_p$  of defects. Weak

collective pinning has been fully developed in the wake of the high- $T_c$  discovery<sup>1,9</sup>, although results have remained qualitative. On the other hand, the theory of strong pinning provides quantitative results, but its development is less advanced. The critical currents<sup>10</sup>, current–voltage characteristics<sup>11,12</sup>,  $ac$ -response<sup>13–15</sup>, and the overall pinning diagram<sup>16,17</sup> have been analyzed and augmented by numerical simulations<sup>18–20</sup>. However, so far

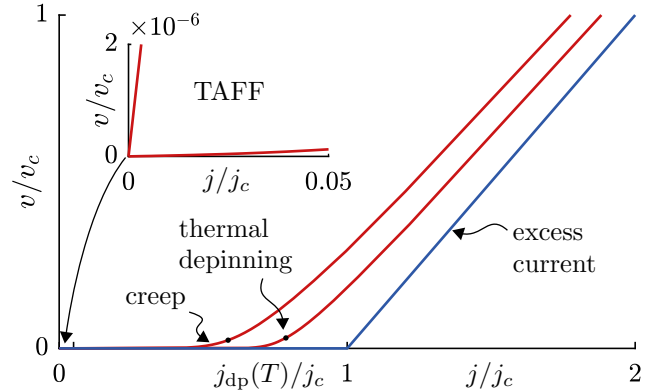


FIG. 1. Current–velocity characteristic of a type II superconductor with strongly pinned vortices and including effects of thermal fluctuation. The  $T = 0$  linear excess-current characteristic (in blue) with its critical current density  $j_c$  is modified due to thermal creep (red curves with  $T/e_p = (0.5, 1) \times 10^{-2}$ ): i) finite temperatures  $T > 0$  shift the linear branch to the left as described by a thermal reduction of  $j_c$  to the depinning current density  $j_{dp}(T) < j_c$ , ii) the characteristic is rounded at the onset of vortex motion near  $j_{dp}(T)$ , and iii) the characteristic turns ohmic at small current densities  $j \rightarrow 0$ , see inset, an effect commonly known as thermally assisted flux flow or TAFF.

no systematic theory including thermal fluctuations has been developed, although important understanding of the creep mechanism can be derived from the work on charge-density wave pinning by Brazovskii, Larkin, and Nattermann<sup>21,22</sup>, see also early work by Fisher<sup>23,24</sup>.

In this paper, we adopt the strong pinning paradigm and present quantitative results on the pinning and creep of vortices in type II superconductors in the presence of thermal fluctuations. Such vortices result from a magnetic field  $\mathbf{H}$  penetrating the superconductor<sup>25–27</sup>, each vortex carrying a quantum of flux  $\phi_0 = hc/2e$  and together forming a lattice of density  $a_0^{-2} = B/\phi_0$  inducing the average magnetic field  $\mathbf{B}$ . The resulting vortex matter is pushed by the current density  $\mathbf{j}$  via the Lorentz-force density  $\mathbf{F}_L = \mathbf{j} \times \mathbf{B}/c$ . The resulting force-velocity characteristic follows from the dissipative force-balance equation

$$\eta v = F_L(j) - F_{\text{pin}}(v, T), \quad (1)$$

where  $\eta \approx BH_{c2}/\rho_n c^2$  denotes the Bardeen-Stephen viscosity (per unit volume,  $H_{c2}$  is the upper-critical field and  $\rho_n$  the normal-state resistivity) and  $F_{\text{pin}}(v, T)$  is the average pinning force density, the quantity of central importance in this paper.

The weak pinning approach provides estimates for the dynamical properties of vortices: the pinning force density  $F_{\text{pin}}$  has been calculated by Larkin and Ovchinnikov<sup>28</sup> and by Schmid and Hauger<sup>29</sup> using a high-velocity perturbative expansion, while the depinning dynamics around  $j_c$  has been studied via renormalization group techniques by Narayan and Fisher<sup>30</sup> and by Chauve *et al.*<sup>31</sup>. On the contrary, the strong pinning scenario produces quantitative results, provided that the density  $n_p$  of defects is small such that they act independently, i.e., the pinning-force density  $F_{\text{pin}} \propto n_p$  is linear in the density of defects (but scales non-trivially in the force  $f_p \sim e_p/\xi$  of individual defects). Pinning is strong if the largest (negative) curvature of the pinning potential  $\partial_R^2 e_p(R)$  wins over the effective vortex stiffness  $\bar{C}$ ; this is expressed in the Labusch criterion<sup>8</sup>  $\kappa = \max_R |\partial_R^2 e_p(R)|/\bar{C} > 1$  characterizing strong pins. The vortex deformation due to an individual pin then exhibits bistable solutions defining pinned and free vortex branches (Fig. 3). Their asymmetric occupation is at the origin of a finite average pinning-force density  $F_{\text{pin}}$  exerted on the vortex lattice by the randomly positioned defects. The determination of its maximal value provides the critical force density<sup>7,8,16</sup>  $F_c$ . The calculation of its dynamical variant  $F_{\text{pin}}(v)$  in the absence of thermal fluctuations<sup>11,12</sup> gives access to the full  $T = 0$  characteristic; this turns out to be of an excess-current form, i.e., the linear flux-flow characteristic of the defect-free superconductor is shifted by a finite critical current density  $j_c$ , see Fig. 1. Note that, although pinning by an individual defect is strong, the small defect density  $n_p$  results in small or moderate pinning forces; hence, strong pinning theory is not necessarily the theory producing highest critical current densities.

In order to account for thermal fluctuations in the average pinning-force density  $F_{\text{pin}}(v, T)$ , we follow Brazovskii and Larkin<sup>21</sup> and use Kramer's rate theory<sup>32</sup> to describe transitions between the pinned and free vortex branches and determine the branch occupation at finite temperatures and velocities. At large velocities but below the (thermal) velocity  $v_{\text{th}} \sim \kappa(T/e_p)v_p$ , finite temperature assists the motion of vortices, diminishes the asymmetry in the vortex branch occupation, and thus reduces the pinning-force density to lie below the critical value  $F_c$ ; here, the depinning velocity  $v_p = f_p/\eta a_0^3$  characterizes the dissipative motion in the defect potential. The critical current density  $j_c$  is reduced to a depinning current density  $j_{\text{dp}}(T)$  separating flat and steep regions of the characteristic, see Fig. 1; to leading order, the relative shift depends on temperature as  $1 - j_{\text{dp}}(T)/j_c \propto (T/e_p)^{2/3}$  and is logarithmically dependent on the density  $n_p$  of defects, see Sec. III B. Beyond depinning, we find a weak dependence of  $F_{\text{pin}}(v, T)$  on the velocity  $v$  and thus recover a close to linear excess-current characteristic, shifted downward in current with respect to the  $T = 0$  result. Hence, contrary to usual expectations, a large pinning-force density as well as thermal creep remain present far beyond the critical current density  $j_c$ , see Ref. [33]. Finally, writing the vortex velocity in the form  $v = v_{\text{th}} e^{-U(j)/T}$ , reminiscent of its thermal origin with  $U(j)$  the activation barrier, we find a decreasing activation barrier  $U(j < j_c) \propto (1 - j/j_c)^{3/2}$  when approaching the depinning region from below. However, the barrier persists well beyond  $j_c$ , where it is characterized by a slow logarithmic variation with the current density  $j$ ,  $U(j \gtrsim j_c) \approx U(j_c) - T \ln[1 + (j - j_c)/(j_c - j_{\text{dp}}(T))]$ , consistent with a linear force-velocity characteristic.

Weak drives  $j$  are characterized by a nearly symmetric occupation of branches, more precisely, an occupation that is shifted linearly in  $j$  with respect to the thermal equilibrium occupation. This results in an ohmic response with exponentially small velocities  $v$ , usually known as TAFF, thermally assisted flux-flow<sup>34</sup>, a specific form of vortex creep at low drive. As implied by its name, the resistivity is thermally assisted, i.e.,  $\rho_{\text{TAFF}} \propto \rho_{\text{ff}} \exp(-U_0/k_B T)$ ,  $\rho_{\text{ff}}$  the flux-flow resistivity, with the finite activation barrier  $U_0$  derived directly from the bistable solutions, see Sec. III C below. As a result, within the framework of strong pinning, the superconductor loses its defining property of dissipation-free current transport. This is quite different as compared with the result of weak collective pinning theory, where barriers diverge  $U(j \rightarrow 0) \propto j^{-\mu}$ , thereby establishing a truly superconducting (glass) state at low drives  $j$ .

Below, we start with a brief review of the strong pinning formalism and show how the interaction of independent defects with the vortex lattice is reduced to a single-pin-single-defect problem involving the effective vortex elasticity  $\bar{C}$ , see Sec. II A. In Sec. III, we extend the analysis to include thermal fluctuations; we discuss creep effects at large drives and velocities in Sec. III B and find the depinning current density  $j_{\text{dp}}(T)$  and the relevant

creep barriers  $U(j)$  in its vicinity. In section III C, we focus on small drives and low velocities and find the ohmic TAFF characteristics with a quantitative prediction of the activation barrier. Finally, in the appendices we provide details of the energy landscape in the marginally- and very strong pinning regime and other technical details of calculations omitted in the main text. In our analytic work, we focus on the relevant limiting cases, small ( $j \rightarrow 0$ ) and large ( $j \sim j_c$ ) drives as well as the limits of marginally strong pinning with  $\kappa \gtrsim 1$  and very strong pinning,  $\kappa \gg 1$ . The new insights on the persistence of pinning and creep beyond the critical drive has been published in a short format in Ref. [33].

## II. FORMALISM

### A. Strong Pinning

In the absence of defects (pins) and thermal fluctuations, our vortex array, aligned along the  $z$ -axis, is arranged in a two-dimensional (2D) hexagonal lattice with equilibrium positions  $\mathbf{R}_\mu = (x_\mu, y_\mu)$ . The presence of strong defects results in deformations of the lattice described by the planar displacement field  $\mathbf{u}_\mu(z)$ . We consider a representative single defect placed in the origin and characterised by a radially symmetric bare pinning potential  $e_p(R) \delta(z)$ , with  $e_p(R)$  decaying on the length  $\sigma$  and  $e_p$  the maximal pinning energy. For a point-like defect, the pinning potential extends over a distance  $R \sim \xi$ ; for a defect of size  $\sigma \sim \xi$ , the energy  $e_p$  is determined by the condensation energy,  $e_p \sim H_c^2 \xi^3$ , see Ref. [14] for more details. Furthermore, we consider a situation where the repulsion between vortices prevents two of them from occupying the same defect<sup>35</sup>, limiting the interaction between vortices and the defect to the single reference vortex  $\mu_0 \equiv 0$  closest to the origin. Such a situation is realized at small and intermediate fields with  $a_0 \gg \xi$  and a not too large pinning energy  $e_p$ . The free energy of this setup then takes the form

$$F[\mathbf{u}] = \int dz e_p[\mathbf{R}_0 + \mathbf{u}_0(z)] \delta(z) + \frac{1}{2} \int \frac{d^3 \mathbf{k}}{(2\pi)^3} u_\alpha(\mathbf{k}) \phi_{\alpha\beta}(\mathbf{k}) u_\beta(-\mathbf{k}), \quad (2)$$

where the first term describes the vortex-defect interaction and the second contributes the elastic energy, expressed through the (symmetric and real) reciprocal-space elastic matrix<sup>8</sup>  $\phi_{\alpha\beta}(\mathbf{k})$ . Here,  $\mathbf{u}_0(z=0) \equiv \mathbf{u}_0$  denotes the tip position of our reference vortex pinned to the defect at the origin. The displacement fields in real and reciprocal space are related through [we decompose

$$\mathbf{r}_\mu = (\mathbf{R}_\mu, z) \text{ and } \mathbf{k} = (\mathbf{K}, k_z)]$$

$$\mathbf{u}(\mathbf{k}) = a_0^2 \int dz \sum_\mu e^{-i\mathbf{k} \cdot \mathbf{x}_\mu} \mathbf{u}_\mu(z), \quad (3)$$

$$\mathbf{u}_\mu(z) = \int \frac{d^3 \mathbf{k}}{(2\pi)^3} e^{i\mathbf{k} \cdot \mathbf{x}_\mu} \mathbf{u}(\mathbf{k}). \quad (4)$$

The integration over  $\mathbf{K}$  is restricted to the 2D Brillouin zone of the vortex lattice,  $K_{\text{BZ}} = 4\pi/a_0^2$  in the circularized approximation, while  $k_z$  is subject to the cutoff  $|k_z| < \pi/\xi$ .

The variation of Eq. (2) with respect to the displacement field  $\delta \mathbf{u}$  provides us with the response

$$\delta F = -f_{p,\alpha}[\mathbf{R}_0 + \mathbf{u}_0] \delta u_{0,\alpha} + \int \frac{d^3 \mathbf{k}}{(2\pi)^3} \delta u_\alpha(\mathbf{k}) \phi_{\alpha\beta}(\mathbf{k}) u_\beta(-\mathbf{k}), \quad (5)$$

where  $f_{p,\alpha} = -\partial e_p / \partial x_\alpha$  denotes the pinning force. Expressing the real-space perturbation  $\delta u_{0,\alpha}$  in the first term through the Fourier modes  $\delta u_\alpha(\mathbf{k})$ , this reads

$$\delta F = \int \frac{d^3 \mathbf{k}}{(2\pi)^3} \delta u_\alpha(\mathbf{k}) \{ -f_{p,\alpha}[\mathbf{R}_0 + \mathbf{u}_0] e^{i\mathbf{K} \cdot \mathbf{R}_0} + \phi_{\alpha\beta}(\mathbf{k}) u_\beta(-\mathbf{k}) \}. \quad (6)$$

For a lattice moving with a steady drift velocity  $\mathbf{v}$ , the asymptotic vortex positions are given by  $\mathbf{R}_\mu(t) = \mathbf{R}_\mu(0) + \mathbf{v}t$ . The full dynamical response of the vortex lattice including time-dependent displacements has to be calculated from the dissipative dynamical equation of motion  $\eta \dot{\mathbf{u}} = -\delta F / \delta \mathbf{u}$  and is addressed in Refs.<sup>11,12</sup>. In the present work, we neglect dynamical effects and assume that the drift velocity is sufficiently small such that the vortex displacement field locally minimizes the energy (2) at any moment of time,  $\delta F / \delta \mathbf{u} = 0$ . The displacement field  $\mathbf{u}$  then depends on time only through the boundary condition, the asymptotic position  $\mathbf{R}_0$  of the reference vortex  $\mu_0 = 0$ , and relates to the pinning force  $\mathbf{f}_p$  via

$$u_\alpha(\mathbf{k}) = G_{\alpha\beta}(\mathbf{k}) f_{p,\beta}[\mathbf{R}_0 + \mathbf{u}_0] e^{-i\mathbf{K} \cdot \mathbf{R}_0} \quad (7)$$

with the Green's function  $G_{\alpha\beta}(\mathbf{k}) = [\phi^{-1}(\mathbf{k})]_{\alpha\beta}$ . Using Eq. (7), we can first solve for  $u_{0,\alpha}$ , the  $\alpha$ -component of  $\mathbf{u}_0$ , and then express the complete displacement field  $\mathbf{u}(\mathbf{k})$  through the tip position  $\mathbf{u}_0$  of the reference vortex. After transformation back to real space, we obtain

$$u_{0,\alpha} = f_{p,\beta}[\mathbf{R}_0 + \mathbf{u}_0] \int \frac{d^3 \mathbf{k}}{(2\pi)^3} G_{\alpha\beta}(\mathbf{k}). \quad (8)$$

We express the last integral through the effective elasticity  $\bar{C}$ ,

$$\bar{C}^{-1} = \frac{1}{2} \int \frac{d^3 \mathbf{k}}{(2\pi)^3} G_{\alpha\alpha}(\mathbf{k}), \quad (9)$$

(with summation over  $\alpha$  implied) and make use of the self-consistent solution of Eq. (8) to obtain the displacement field expressed through the amplitude  $u_{0,\beta}$ ,

$$u_\alpha(\mathbf{k}) = \bar{C} G_{\alpha\beta}(\mathbf{k}) u_{0,\beta} e^{-i\mathbf{k}\cdot\mathbf{R}_0}. \quad (10)$$

Inserting this result back into Eq. (2), we obtain a simple expression for the free energy  $F[\mathbf{u}] \rightarrow e_{\text{pin}}(\mathbf{R}_0, \mathbf{u}_0)$  for our specific configuration with the tip at  $z = 0$  of the vortex  $\mu_0 = 0$  displaced by  $\mathbf{u}_0$  from its asymptotic position  $\mathbf{R}_0$  due to the action of the defect,

$$e_{\text{pin}}(\mathbf{R}_0, \mathbf{u}_0) = e_p[\mathbf{R}_0 + \mathbf{u}_0] \quad (11)$$

$$+ \frac{\bar{C}^2}{2} \int \frac{d^3\mathbf{k}}{(2\pi)^3} G_{\alpha\beta}(\mathbf{k}) u_{0,\beta} \phi_{\alpha\gamma}(\mathbf{k}) G_{\gamma\delta}(-\mathbf{k}) u_{0,\delta} \\ = e_p[\mathbf{R}_0 + \mathbf{u}_0] + \frac{\bar{C}}{2} \mathbf{u}_0^2. \quad (12)$$

Next, we choose the vortex position along the  $x$ -axis,  $\mathbf{R}_0 = x \mathbf{e}_x$  and assume a radially symmetric pin, implying that  $\mathbf{u}_0 = u \mathbf{e}_x$ ; expressing the effective free energy in Eq. (12) in terms of the vortex tip coordinate  $r = x + u$ , we arrive at the simplified effective pinning energy

$$e_{\text{pin}}(x; r) = \frac{1}{2} \bar{C} (r - x)^2 + e_p(r). \quad (13)$$

The effective pinning energy  $e_{\text{pin}}(x; r)$  involves the bare pinning potential  $e_p(r)$  augmented by the elastic deformation energy of the vortex in the form of a parabolic potential centered at  $r = x$ , see Fig. 2, with a curvature given by the effective vortex lattice elasticity  $\bar{C}$ . The latter can be expressed through the compression, tilt and shear elastic moduli known from elasticity theory<sup>1,14</sup>,  $\bar{C} = \gamma(a_0^2/\lambda)[c_{66}c_{44}(\mathbf{k} = 0)]^{1/2}$ ; the numerical  $\gamma$  depends on the chosen approximations, see Refs.<sup>12,35</sup>. The simple estimate  $\bar{C} \sim \sqrt{\varepsilon_0 \varepsilon_\ell}/a_0$ , where  $\varepsilon_\ell = \varepsilon_0 \ln(a_0/\xi)$ , is governed by the value of the vortex line energy  $\varepsilon_0 = (\phi_0/4\pi\lambda)^2$ .

If pinning is sufficiently strong, i.e.,  $e_p(r)$  is sufficiently deep, the total free energy  $e_{\text{pin}}(x; r)$  has two minima within a finite range  $|x| \in [x_-, x_+]$  of asymptotic vortex positions  $x$ . Minima appear or vanish whenever the total pinning energy develops an inflection point,  $\partial^2 e_{\text{pin}}/\partial r^2 = \bar{C} - f'_p(r) = 0$ . This requires that the condition

$$\kappa = \frac{\max_r f'_p(r)}{\bar{C}} > 1, \quad (14)$$

the so-called Labusch criterion<sup>8</sup>, is fulfilled, see bottom of Fig. 2. The value  $\kappa = 1$  marks the transition between weak pinning with a unique vortex configuration and the strong-pinning situation where the vortex can choose between two alternative configurations, a pinned and a free one, whenever its asymptotic position  $|x|$  resides in the interval  $[x_-, x_+]$ . The two local minima  $r_p(x)$  and  $r_f(x)$  are obtained from minimizing  $e_{\text{pin}}(x; r)$  with respect to  $r$  at fixed  $x$ ,

$$\bar{C}(r - x) = f_p(r). \quad (15)$$

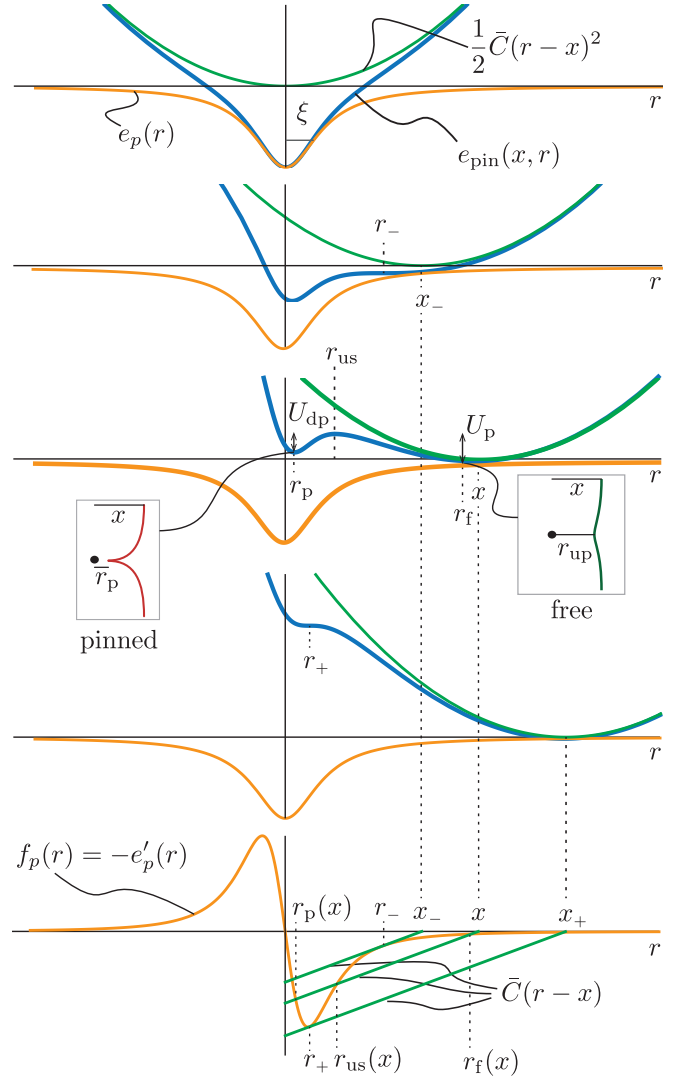


FIG. 2. Effective pinning energy  $e_{\text{pin}}(x; r)$  versus  $r$  for four different asymptotic vortex positions  $x$ ,  $0 \leq x \leq x_+$ . We assume a Lorentzian defect with a potential  $e_p(R) = -e_p/(1 + R^2/2\xi^2)$  and a Labusch parameter  $\kappa = 5$ . Two local minima at  $r_p$  and  $r_f$  appear for  $x_- < x < x_+$  and are separated by the local maximum at  $r_{\text{us}}$  defining the barrier  $U_{\text{dp}}(x)$  for depinning (the barrier to escape the pin) and the barrier  $U_p(x)$  for pinning (or jumping into the pin). Bottom: Minimizing  $e_{\text{pin}}(x; r)$  with respect to the tip position  $r$  at fixed asymptotic position  $x$  corresponds to solving the self-consistency equation  $\bar{C}(r - x) = f_p(r)$ , see (15), here done graphically. Multiple solutions  $r_i(x)$ , ( $i = p, f, us$ ), show up if the slope  $\bar{C}$  is smaller than the maximum slope of  $f_p(r)$ , what corresponds to a Labusch parameter  $\kappa > 1$ .

The local maximum at  $r_{\text{us}}(x)$  is an unstable solution that plays an important role in the context of creep, see below.

Fig. 3 shows the multi-valued energy landscape with the three branches  $e_{\text{pin}}^p(x)$ ,  $e_{\text{pin}}^f(x)$ , and  $e_{\text{pin}}^{\text{us}}(x)$  corresponding to the extremal solutions,  $e_{\text{pin}}^i(x) = e_{\text{pin}}[x; r_i(x)]$ ; three of them coexist in the two intervals where  $|x| \in [x_-, x_+]$ , while outside those regions only



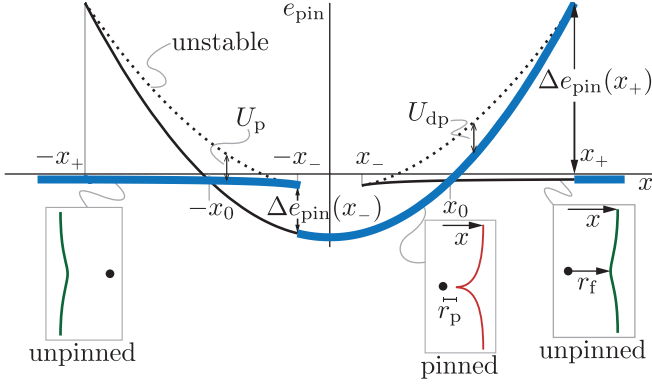


FIG. 3. Multivalued energy landscape for a strong defect. Within the regions  $|x| \in [x_-, x_+]$ , pinned and free equilibrium positions show up with different locations  $r_p(x)$  and  $r_f(x)$  of the vortex tips either close to or away from the defect; they define the energies  $e_{\text{pin}}^p(x)$  and  $e_{\text{pin}}^f(x)$  of the pinned (nearly parabolic) and free (nearly flat) branches. In addition, an unstable extremum at  $r_{\text{us}}(x)$ , see Fig. 2, maximises the pinning energy (dotted) unstable branch  $e_{\text{pin}}^{\text{us}}$  and defines the energy barriers connecting pinned and free branches. Thick blue curves denote the occupation of branches in the critical state realised for  $T = 0$ . The pinning force is proportional to the sum of jumps  $\Delta e_{\text{pin}}(x_+)$ ,  $\Delta e_{\text{pin}}(x_-)$  in the energy landscape.

one solution is realized. The total pinning force exerted on a moving vortex is derived from this energy landscape, with the pinning force acting on a vortex given by  $f_{\text{pin}}(x) = -de_{\text{pin}}(x)/dx$ . As this force differs when evaluated in the pinned and free branches, it is the occupation of these branches that determines the total pinning-force density acting on the vortex system. The pinned and free branches in the pinning-energy landscape are separated by an energy barrier. The *depinning* barrier  $U_{\text{dp}}(x) = e_{\text{pin}}^{\text{us}}(x) - e_{\text{pin}}^p(x)$  has to be overcome for transitions to the free branch, while the *pinning* barrier  $U_p(x) = e_{\text{pin}}^{\text{us}}(x) - e_{\text{pin}}^f(x)$  is relevant for jumps into the pin, i.e., the transitions to the pinned branch.

Unfortunately, no closed expressions for the branches  $e_{\text{pin}}^i(x)$  can be given since the equilibrium equation (15) fixing  $r(x)$  is in general not solvable analytically. Progress can be made in the limits of marginally strong pinning with  $\kappa - 1 \ll 1$  or for very strong pinning  $\kappa \gg 1$ . In the first case the slope  $\bar{C}$  is close to the maximum slope of  $f_p(r)$  and the energy branches can be derived from a cubic expansion of  $f_p(r)$  around the point  $r_m$  of maximum slope,  $f_p'(r_m) = \kappa\bar{C}$ . For very strong pinning, the slope  $\bar{C}$  is small compared to  $f_p'(r_m)$  and the pinned and unstable solutions are obtained by analyzing the tail of  $f_p(r)$ . We will assume an algebraically decaying potential,  $e_p(r \gg \xi) \sim e_p(\xi/r)^n$  such that the pinning force  $f_p(r \gg \xi) \sim f_p(\xi/r)^{n-1}$  with  $f_p \sim e_p/\xi$ , in order to make analytic progress in this situation.

The boundaries  $x_{\pm}$  of the multi-valued interval are found by first determining the critical tip positions  $r_{\pm}$  from the condition  $f_p'(r_{\pm}) = \bar{C}$  for the appearance of inflection points in  $e_{\text{pin}}(x; r)$  and then deriving the asso-

ciated asymptotic position  $x_{\pm}$  from the equilibrium condition Eq. (15), see also Fig. 2. For marginally strong pinning, we find that (see Ref. [16], Appendix A and B for the derivation)

$$r_{\pm} - r_m \sim \mp(\kappa - 1)^{1/2}\xi, \quad (16)$$

$$x_{\pm} - x_m \sim \pm(\kappa - 1)^{3/2}\xi, \quad (17)$$

where  $r_m \lesssim x_m \sim \xi$ . Note that  $x_m$  coincides with the branch crossing point  $x_0$ ,  $x_m = x_0$ . For very strong pinning,  $r_-$  resides on the tail of the pinning potential, while  $r_+$  is located near the maximum force,

$$r_- \sim \kappa^{1/(n+2)}\xi, \quad r_+ \sim \xi. \quad (18)$$

The associated asymptotic positions are largely different, see also Fig. 2,

$$x_- \sim \kappa^{1/(n+2)}\xi, \quad x_+ \sim \kappa\xi. \quad (19)$$

Finally, the branch crossing point is located at a position where the free and pinned branches have the same energies,  $\bar{C}x_0^2/2 \approx e_p$ , implying that  $x_0 \approx \sqrt{2e_p/\bar{C}} \sim \kappa^{1/2}\xi$ .

The free-energy landscape in Fig. 3 has much in common with the one appearing in the phenomenological theory of a first-order phase transition in thermodynamic systems, e.g., the Gibb's energy  $g(p, T)$  of the Van der Waal's theory of the gas-liquid transition or the energy  $g(h, T)$  of a magnetic transition. In developing this analogy, we can identify  $\bar{C}r$  with the volume  $V$  and  $\bar{C}$  (or the inverse Labusch parameter  $1/\kappa$ ) with the reduced temperature  $\tau = T/T_c$ . Expanding  $e_{\text{pin}}(x; r) = e_p(r) + \bar{C}r^2/2 - \bar{C}rx + \bar{C}x^2/2$ , we can identify the energy  $e_p(r) + \bar{C}r^2/2$  with the free energy  $f(V, \tau)$ . If  $x$  is identified with pressure  $p$ , then  $e_{\text{pin}}(x; r)$  is (up to the constant term  $\bar{C}x^2/2$ ) equivalent to the Gibb's energy  $g = f - pV$ . Minimizing  $e_{\text{pin}}$  with respect to  $r$  for fixed  $x$  and  $\bar{C}$  corresponds to minimizing  $g$  with respect to  $V$  for fixed  $p$  and  $T$  and provides the (metastable) equilibrium states (note that  $\bar{C}r$  and  $V$  play the roles of constraint parameters). The barrier separating the minima in the thermodynamic system are relevant in the description of the hysteretic transition and nucleation phenomena—here, the analogous barriers describe thermal transitions between pinned and free states and thus are relevant in the description of thermal creep.

## B. Pinning force

The average pinning force per defect acting on the vortex system is obtained by position-averaging the force between a defect and its nearest vortex while accounting for the random positions of the defects in the material. Driving the vortices in the positive  $x$ -direction results in an average force  $-\langle f_{\text{pin}} \rangle < 0$  per defect (in accordance with (1), we choose  $\langle F_{\text{pin}} \rangle$  and hence  $\langle f_{\text{pin}} \rangle$  to be positive). The instantaneous force acting on a vortex with asymptotic position  $x$  is different for pinned and free states. Let

$p(x)$  be the occupation probability of the pinned branch; the occupation probability for the free branch then is  $1 - p(x)$ . For a vortex passing centrally through the defect, the average pinning force is given by the position and occupation average

$$\langle f_{\text{pin}} \rangle = -\frac{1}{a_0} \int_{-a_0/2}^{a_0/2} dx [p f_{\text{pin}}^{\text{p}} + (1 - p) f_{\text{pin}}^{\text{f}}](x), \quad (20)$$

with  $f_{\text{pin}}^{\text{p,f}}(x) = -de_{\text{pin}}^{\text{p,f}}(x)/dx$  denoting the pinning forces on the pinned and free branches. For  $|x| < x_-$  only the pinned branch is available, while for  $|x| > x_+$  the occupation is restricted to the free branch; hence, we set  $p(x) = 1$  and  $p(x) = 0$ , respectively, in those two regions. The integration is restricted to  $|x| < a_0/2$  due to the vortex lattice periodicity. The antisymmetric force with  $f_{\text{pin}}^{\text{p,f}}(x) = -f_{\text{pin}}^{\text{p,f}}(-x)$  allows to write the previous equation in the form

$$\langle f_{\text{pin}} \rangle = -\frac{1}{a_0} \int_{I_{\text{mv}}} dx p(x) \Delta f_{\text{pin}}(x) \quad (21)$$

with  $\Delta f_{\text{pin}} = f_{\text{pin}}^{\text{p}} - f_{\text{pin}}^{\text{f}}$  and the integration restricted to the multivalued intervals  $I_{\text{mv}} = [-x_+, -x_-] \cup [x_-, x_+]$ .

The  $T = 0$  branch occupation for vortices driven along the positive  $x$ -axis is shown in Fig. 3, see blue solid lines. An individual vortex approaches the defect on the free branch and remains there until  $-x_-$ , even though the pinned branch becomes energetically more favorable at the branch crossing point  $-x_0 < -x_-$ . The vortex becomes pinned at  $-x_-$  when the *pinning* barrier  $U_{\text{p}}$  vanishes and stays on the pinned branch until  $x_+$ , where it jumps again to the unpinned branch, this time due to the vanishing of the *depinning* barrier  $U_{\text{dp}}$ . The occupation then can be written through the Heaviside step function  $\Theta(x)$ ,

$$p_c(x) = \Theta(x + x_-) - \Theta(x - x_+), \quad (22)$$

and using  $f_{\text{pin}} = -\partial_x e_{\text{pin}}$  in Eq. (20), we find that

$$\langle f_{\text{pin}} \rangle = \frac{\Delta e_c}{a_0} \quad (23)$$

with  $\Delta e_c = \Delta e_{\text{pin}}(x_+) - \Delta e_{\text{pin}}(-x_-)$  and  $\Delta e_{\text{pin}} = e_{\text{pin}}^{\text{p}} - e_{\text{pin}}^{\text{f}}$ . Note that  $\Delta e_{\text{pin}}(-x_-) = \Delta e_{\text{pin}}(x_-) < 0$  and  $\Delta e_c$  thus corresponds to the sum of the energy jumps in the multivalued energy landscape evaluated at the end points of the multivalued intervals.

Estimates for the jumps  $\Delta e_{\text{pin}}(x_{\pm})$  are derived in Appendix A and B, see also Refs. <sup>8,16</sup>. For marginally strong pinning, one finds that

$$\Delta e_{\text{pin}}(x_{\pm}) \sim \bar{C} \xi^2 (\kappa - 1)^2 \quad (24)$$

while for very strong pinning

$$\Delta e_{\text{pin}}(x_{\pm}) \approx \frac{\bar{C}}{2} x_{\pm}^2, \quad (25)$$

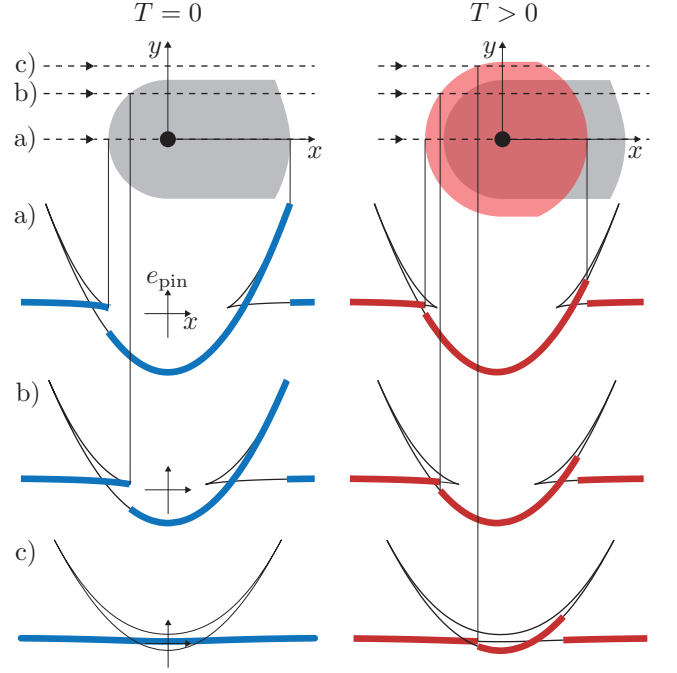


FIG. 4. Pinning of vortices passing the defect at transverse distances  $y = 0$  (a),  $y = 0.8x_-$  (b), and  $y = 1.2x_-$  (c) for  $T = 0$  (blue, left) and finite temperatures (red, right). The corresponding pinning energy landscapes  $e_{\text{pin}}^i(x, y)$  are plotted for the Lorentzian pinning potential and  $\kappa = 5$ . At  $T = 0$ , vortices are pinned whenever they enter the defect trapping area (along the grey half circle of radius  $x_-$ , where the free and unstable branches merge and disappear such that  $U_{\text{p}}(x, y) = 0$ ). In case (c) the vortex trajectory lies outside the trapping area and vortices always stay on the free branch, which is available all the way along the vortex trajectory; the pinning force vanishes in this case. At finite temperature  $T > 0$ , the transitions between the free and pinned branches are realized at a radial distance  $x_{\pm}^{\text{jp}} > x_-$  from the pinning centre. Due to thermal activation, vortices can overcome the barrier separating free and pinned branches and occupy the pinned branch even for  $y > x_-$ , resulting in a non-vanishing average pinning force in the extended region  $y < x_-^{\text{jp}}$  (light red).

in particular, using Eq. (19), we find that  $\Delta e_{\text{pin}}(x_+) \sim \bar{C} \kappa^2 \xi^2 \sim \kappa e_p$  is large compared to  $\Delta e_{\text{pin}}(x_-) \sim \kappa^{1/(n+2)} e_p$ .

Above, we have considered the situation where the vortex impacts straight on the defect center. For those vortices passing the defect at a finite transverse distance  $y$  (Fig. 4), the effective pinning energy is given by  $e_{\text{pin}}(\mathbf{R}, \mathbf{r}) = \frac{1}{2} \bar{C} (\mathbf{R} - \mathbf{r})^2 + e_p(\mathbf{r})$ , where  $\mathbf{R}$  and  $\mathbf{r}$  denote the asymptotic- and tip-position of the vortex line, see Eq. (12) (we drop the index  $\mu_0 = 0$ ). The equilibrium condition  $\nabla_{\mathbf{r}} e_{\text{pin}} = 0$  yields the solutions  $\mathbf{r}_i(\mathbf{R})$ ,  $i = \text{f, p, u}$  for the free, pinned, and unstable branches. For a radially symmetric pinning potential, we have  $e_p(\mathbf{r}) = e_p(r)$  and the equilibrium condition is satisfied for the radial geometry  $\mathbf{r} \parallel \mathbf{R}$ . The energy is then brought to the same form as in Eq. (13), albeit

with the replacement  $x \rightarrow |\mathbf{R}| = \sqrt{x^2 + y^2}$ . Evaluating  $e_{\text{pin}}^i(\mathbf{R}) = e_{\text{pin}}[\mathbf{R}, \mathbf{r}_i(\mathbf{R})]$  provides us with the energies of the various branches in the multivalued energy landscape,  $i = \text{f, p, us}$ ,

$$e_{\text{pin}}^i(\mathbf{R}) = e_{\text{pin}}^i(x, y) = e_{\text{pin}}^i(\sqrt{x^2 + y^2}, 0). \quad (26)$$

The energy landscape is plotted in Fig. 4 for three impact parameters  $y = 0$ ,  $y = 0.8x_-$ , and  $y = 1.2x_-$ . Eq. (26) shows that the shape of the energy landscape at finite impact parameter  $y$  is similar to the one at  $y = 0$  with an excluded region  $|x| < y$ . In particular, the minimal energy of the pinned branch satisfies  $e_{\text{pin}}^{\text{p}}(0, y) = e_{\text{pin}}^{\text{p}}(y, 0) > e_{\text{pin}}^{\text{p}}(0, 0)$ . For a large impact parameter  $y > x_-$  (the situation with  $y = 1.2x_-$  is shown in Fig. 4) the free branch never terminates, implying that such a vortex is never trapped at  $T = 0$ . On the other hand, vortices hitting the defect with a finite impact parameter  $y < x_-$  are trapped onto the defect at the radial distance  $R = x_-$  and released back to the free branch at a radial distance  $R = x_+$ , hence the vortex remains pinned over the finite interval  $x \in [-\sqrt{x_-^2 - y^2}, \sqrt{x_+^2 - y^2}]$ , with  $x$  the direction of drive, and for all  $y < t_{\perp} = x_-$ ; we call  $t_{\perp}$  the transverse trapping length. The average pinning force along the  $x$ -direction is once more given by Eq. (20), but with the pinning forces replaced by  $f_{\text{pin}}^{\text{p,f}}(x) \rightarrow f_{\text{pin}}^{\text{p,f}}(x, y) = -\partial_x e_{\text{pin}}^{\text{p,f}}(x, y) = -\partial_x e_{\text{pin}}^{\text{p,f}}(\sqrt{x^2 + y^2}, 0)$  and the jumps in the occupation (22) now appearing at  $\sqrt{x_-^2 - y^2}$  and  $\sqrt{x_+^2 - y^2}$ . A simple calculation then shows, that the average force  $\langle f_{\text{pin}}(y) \rangle$  contributed by a vortex with an impact parameter  $y < x_-$  is identical with the result (23). While vortices passing the defect at larger distances cannot get trapped at zero temperature, fluctuations at finite temperature will render such processes statistically possible, see Sec. III B 3 below.

Combining the above results, we can determine the average pinning force density for a finite density of defects by multiplying the average pinning force (23) with the fraction  $2x_-/a_0$  of trajectories that are trapped by one defect and the density  $n_p$  of independently acting defects; including a minus sign in order to respect our definition of pinning force density in the equation of motion (1), we obtain the critical force density

$$F_c = n_p \frac{2x_-}{a_0} \frac{\Delta e_c}{a_0}. \quad (27)$$

Collecting the various factors from above, we obtain the estimates

$$F_c \sim (\xi/a_0)^2 n_p f_p (\kappa - 1)^2 \quad (28)$$

and

$$F_c \sim (\xi/a_0)^2 n_p f_p \kappa^{(n+3)/(n+2)} \quad (29)$$

in the marginally strong and very strong pinning limits, respectively. Quite often, these results are written

through the trapping area<sup>10,16</sup>  $S_{\text{trap}}$ ,

$$S_{\text{trap}} = 2x_-(x_+ + x_-), \quad F_c \sim \frac{S_{\text{trap}}}{a_0^2} n_p f_p, \quad (30)$$

which assumes values  $S_{\text{trap}} \sim \xi^2$  and  $S_{\text{trap}} \sim \kappa^{(n+3)/(n+2)} \xi^2$  at marginally strong and very strong pinning. For a rapidly decaying pinning potential (with a large value of  $n$ ), the trapping area, critical force density, and critical current density scale like  $S_{\text{trap}} \propto 1/\sqrt{B}$ ,  $F_c \propto \sqrt{B}$ , and  $j_c \propto 1/\sqrt{B}$ ; such a field dependence (cut off at small fields when strong pinning becomes 1D, single-vortex type, see Ref. [16]) is often taken as a signature for strong pinning.

The critical state occupation  $p_c(x)$  in (22) is the one maximizing the pinning force. If the applied force density  $F_L$  exceeds  $F_c$ , the vortex lattice moves with drift velocity as given through the dissipative force balance equation  $\eta v = F_L - F_c$ . The dynamical pinning force  $F_{\text{pin}}(v)$  changes on a scale  $v_p = f_p/a_0^3 \eta \gg v_c = F_c/\eta$  and has been calculated at  $T = 0$  in Refs.<sup>11,12</sup>; below, we focus on the calculation of  $F_{\text{pin}}(v, T)$  at finite temperatures  $T$  but small velocities  $v \ll v_p$ , where the dynamical motion of the vortex through the pin can be neglected, and derive the thermally renormalized force-velocity characteristic.

### III. THERMAL CREEP

We start with a short qualitative overview of thermal creep effects at large and small velocities before deriving precise expressions for the two limits.

#### A. Qualitative overview

At finite temperatures  $T > 0$ , one has to account for thermal fluctuations in the determination of the branch occupation as vortices can jump between branches by overcoming the activation barrier; the same physics appears in the context of pinned charge density waves, see Refs.<sup>21,22</sup>. We find the pinned branch occupation  $p(x)$  through solving the rate equation derived from Kramers' theory<sup>32</sup> (we set  $k_B = 1$  from now on),

$$\frac{dp}{dt} = v \frac{dp}{dx} = -\omega_p e^{-U_{\text{ap}}/T} p + \omega_f e^{-U_p/T} (1 - p). \quad (31)$$

This rate equation accounts for the depinning of vortices via the activation barrier  $U_{\text{dp}}(x)$  as well as the filling of the pinned branch due to transitions over the barrier  $U_p(x)$ . The steady-state probabilities depend on the time  $t$  only through the coordinate  $x$  and thus we have replaced the total derivative by  $d/dt = v d/dx$ . The frequencies  $\omega_p(x)$  and  $\omega_f(x)$  can be understood as the number of attempts per unit of time made by a vortex to escape from its current, pinned or free, state. The success probability of such attempts is exponentially small in

the activation barrier. We calculate the barriers and attempt frequencies later in Sec. III B from a ‘microscopic’ theory.

Focusing on the high- and low-velocity regimes with qualitatively distinct solutions of the rate equation (31) provides us with a first understanding of the problem. The velocity  $v_{\text{th}} = \omega_p T / \partial_x U_{\text{dp}}$  derived below, see Eqs. (36) and (62), sets the scale below which thermal effects modify the  $T = 0$  excess-current characteristic; above  $v_{\text{th}}$ , the  $T > 0$  characteristic smoothly joins the one at  $T = 0$ . The high-velocity regime  $v > v_{\text{th}} e^{-U_0/T}$ , with  $U_0$  the maximal activation barrier located at the branch crossing point  $x_0$ , see Fig. 3, is characterized by an occupation  $p(x)$  of a shape similar to the one of the critical state, but with the transitions between branches realized close to the thermally renormalized jump points  $x_{\pm}^{\text{jp}}(v, T)$ , see Fig. 6. Ignoring the finite width  $\ell_p$  and  $\ell_{\text{dp}}$  of these jumps, we can write  $p(x) \approx \Theta(x - x_-^{\text{jp}}) - \Theta(x - x_+^{\text{jp}})$  and express the pinning force density through the thermally renormalized jumps in the energy landscape

$$F_{\text{pin}}(v, T) = n_p \frac{2x_-^{\text{jp}}}{a_0} \frac{\Delta e_{\text{pin}}^{\text{tot}}(v, T)}{a_0}, \quad (32)$$

where

$$\Delta e_{\text{pin}}^{\text{tot}}(v, T) = \Delta e_{\text{pin}}(x_+^{\text{jp}}) - \Delta e_{\text{pin}}(-x_-^{\text{jp}}) > 0. \quad (33)$$

The jump location  $x_+^{\text{jp}}$  follows from the following consideration (a corresponding analysis provides the location  $-x_-^{\text{jp}}$ , see below): Close to the jump at  $x_+^{\text{jp}}$ , the occupation dynamics is dominated by the smaller depinning barrier  $U_{\text{dp}} < U_p$  and the second term on the right hand side of the rate equation (31) can be ignored. The rate equation then takes the simple form  $\partial_x p = -p/\ell_{\text{dp}}$ , with

$$\ell_{\text{dp}}(x) = \frac{v}{\omega_p} e^{U_{\text{dp}}(x)/T} \quad (34)$$

defining the depinning length at the position  $x > x_0$ , telling us over what distance the vortex will transit from the pinned to the free branch. The depinning length  $\ell_{\text{dp}}(x)$  is large near  $x_0$  where the barrier  $U_{\text{dp}}$  is large and decreases rapidly with increasing  $x$  due to the decreasing barrier  $U_{\text{dp}}$ . The transition to the lower (free) state appears at the position  $x_+^{\text{jp}}$  where the vortex can escape the pin while itself moving a distance  $\ell_{\text{dp}}(x)$ , implying that the relative change in  $\ell_{\text{dp}}(x)$  over the distance  $\ell_{\text{dp}}(x)$  should be of order unity. With the help of Eq. (34), we can reexpress the corresponding condition  $|\partial_x \ell_{\text{dp}}(x)|_{x_+^{\text{jp}}} \approx 1$  in the form

$$\ell_{\text{dp}}(x_+^{\text{jp}}) \approx \frac{T}{U'_{\text{dp}}(x_+^{\text{jp}})}, \quad (35)$$

where we focus on the main  $x$ -dependence in the exponent and denote the space derivative with a prime,  $U'_{\text{dp}} \equiv \partial_x U_{\text{dp}}$ . At the maximal value  $x_+^{\text{jp}} = x_+$ , the barrier  $U_{\text{dp}}(x_+)$  vanishes and we reach the maximal velocity

$v_{\text{th}}$ ,

$$v_{\text{th}} = \frac{\omega_p T}{U'_{\text{dp}}} \Big|_{x_+}, \quad (36)$$

where the thermal characteristic goes over into the  $T = 0$  excess-current characteristic. From the condition (35) and using Eq. (36), we find that the relevant depinning barrier  $U_{\text{dp}}(x_+^{\text{jp}})$  can be written in the form

$$U_{\text{dp}}(x_+^{\text{jp}}) \approx T \ln(v_{\text{th}}/v), \quad (37)$$

where we have approximated  $[U'_{\text{dp}}/\omega_{\text{dp}}](x_+^{\text{jp}})$  by its value at  $x_+$ . Similar results apply for the jump at  $-x_-^{\text{jp}}$  and are quantitatively derived below, see Sec. III B. Given the barriers  $U_{\text{dp}}(x)$  (and  $U_p(x)$ ) for a specific defect potential, we can solve Eq. (37) for  $x_+^{\text{jp}}(v)$  (and similar for  $-x_-^{\text{jp}}(v)$ ) and using the results in the definition of the energy jump Eq. (33) leads to the velocity- and temperature-dependent pinning force density. We cast the final result (see Sec. III B for details) in the form

$$F_{\text{pin}}(v, T) = F_c \left[ 1 - g(\kappa) \left( \frac{T}{e_p} \log \frac{v_{\text{th}}}{v} \right)^{2/3} \right], \quad (38)$$

with  $g(\kappa)$  a factor of order unity that can be derived as a function of pinning strength  $\kappa$  for any given defect potential  $e_p(r)$ .

A different approach has to be used in solving the rate equation for small velocities  $v < v_{\text{TAF}} = v_{\text{th}} e^{-U_0/T}$ . Starting from the above analysis and decreasing the velocity  $v$ , the jump positions  $x_{\pm}^{\text{jp}}$  approach the branch crossing point  $x_0$  and the activation barriers increase towards their maximum  $U_0 = U_{\text{dp}}(x_0) = U_p(x_0)$ , see Fig. 3. At  $x_0$ , the renormalized energy jumps  $\Delta e_{\text{pin}}(x_{\pm}^{\text{jp}} \rightarrow x_0)$  vanish and Eq. (32), providing a vanishing pinning force, can no longer be used. In this limit, a good starting point for our analysis is the equilibrium distribution obtained by setting  $v = 0$  in the rate equation (31).

$$p_{\text{eq}}(x) = \frac{\omega_f e^{-U_p/T}}{\omega_p e^{-U_{\text{dp}}/T} + \omega_f e^{-U_p/T}} = \frac{\ell_{\text{dp}}(x)}{\ell_{\text{dp}}(x) + \ell_p(x)} \quad (39)$$

with  $\ell_p = (v/\omega_f) e^{U_p/T}$  defining the local relaxation distance for the case of pinning. The expression Eq. (39) is valid away from the endpoints of the multi-valued interval where barriers vanish. The rate equation then can be cast into the form

$$\begin{aligned} \frac{dp}{dx} &= \frac{1}{v} (p_{\text{eq}} - p) (\omega_p e^{-U_{\text{dp}}/T} + \omega_f e^{-U_p/T}) \\ &= \frac{p_{\text{eq}}(x) - p}{\ell_{\text{eq}}(x)}, \end{aligned} \quad (40)$$

where the equilibrium relaxation distance  $\ell_{\text{eq}}$ ,

$$\ell_{\text{eq}}(x) = [\ell_p(x)^{-1} + \ell_{\text{dp}}(x)^{-1}]^{-1}, \quad (41)$$

includes processes that connect both pinned and free branches. Treating  $v$  as a small parameter, we find that the solution of the rate equation is given by the shifted equilibrium distribution,  $p(x) \approx p_{\text{eq}}(x) - \ell_{\text{eq}}(x)p'_{\text{eq}}(x) \approx p_{\text{eq}}[x - \ell_{\text{eq}}(x)]$ . Assuming similar scales  $\omega_p \sim \omega_f$  and  $|U'_{\text{dp}}| \sim U'_p$ , we obtain a simple estimate for the equilibrium relaxation length in the form  $\ell_{\text{eq}}(x_0) \sim (v/\omega_p)e^{U_0/T}$  and the condition  $v \ll v_{\text{TAFf}}$  defining the low-velocity regime is then equivalent to  $\ell_{\text{eq}}(x_0) \ll T/|U'_{\text{dp}}|$  implying that the shift  $\ell_{\text{eq}}(x)$  is small compared to the scale of variations in  $p_{\text{eq}}(x)$ . Our low-velocity analysis improves on the work by Brazovskii, Larkin, and Nattermann (BLN)<sup>21,22</sup> discussing thermal effects on the pinning of charged density waves that exhibits similar bistable solutions as found here. In their analysis, the smooth variation in the equilibrium distribution is ignored, what results in a different shift scale  $\ell_{\text{eq}}(x_0)$ , see Sec. III C for further details.

The equilibrium occupation  $p_{\text{eq}}(x)$  is symmetric and thus yields no average pinning force, allowing us to rewrite Eq. (21) as

$$\langle f_{\text{pin}} \rangle = -\frac{1}{a_0} \int_{I_{\text{mw}}} dx (p - p_{\text{eq}}) \Delta f_{\text{pin}} \quad (42)$$

$$\approx \frac{1}{a_0} \int_{I_{\text{mw}}} dx \ell_{\text{eq}}(x) p'_{\text{eq}}(x) \Delta f_{\text{pin}}. \quad (43)$$

Hence, the pinning force depends linearly on  $v$  for small velocities. A detailed analysis (see Sec. III C) shows that the average pinning-force  $\langle f_{\text{pin}} \rangle$  has a non-trivial dependence on the transverse distance, reaching its maximum value given by Eq. (43) at  $y = 0$  and vanishing at  $y = x_0$ . This results in an additional numerical prefactor  $\alpha = \pi/4$  in the formula for the average pinning force density  $F_{\text{pin}}(v, T) = \alpha n_p (2x_0/a_0) \langle f_{\text{pin}} \rangle$ . Carrying out the integration in Eq. (43) yields a quantitative result for the pinning-force density at small velocities,

$$F_{\text{pin}}(v, T) = h(\kappa) n_p a_0 \xi^2 e^{U_0/T} \eta v \quad (44)$$

with a  $\kappa$ -dependent factor  $h(\kappa)$ . The linear dependence  $F_{\text{pin}} \propto v$  then immediately implies an ohmic characteristic at small drive  $j \rightarrow 0$ ; the exponential  $\propto e^{U_0/T}$  leads to the reduced flow velocity that is at the origin of the name TAFf, thermally assisted flux flow<sup>34</sup>.

The results outlined above can be compared with those obtained from a numerical analysis. Taking into account the  $y$ -dependence of the frequency factors and barriers in the rate equation (31), one can solve numerically for the occupation probability  $p(x, y)$ . The average pinning-force density then follows from a modified equation (21),

$$F_{\text{pin}} = -n_p \int \frac{dx dy}{a_0^2} p(x, y) \Delta f_{\text{pin}}(x, y) \quad (45)$$

with  $\Delta f_{\text{pin}}(x, y) = f_{\text{pin}}^p(x, y) - f_{\text{pin}}^f(x, y)$  and the integration covering a unit cell of the vortex lattice. We present the numerical results in the form of a current-velocity

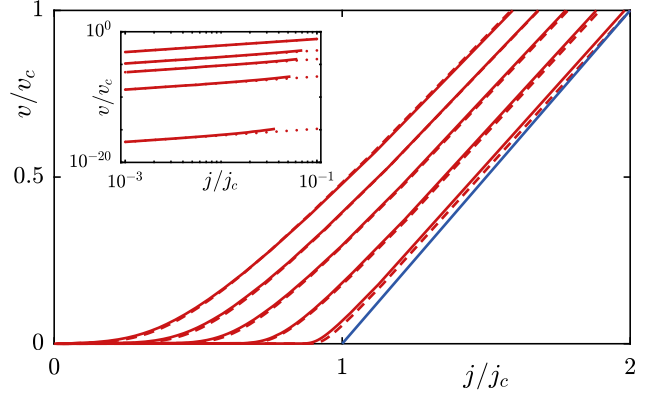


FIG. 5. The current-velocity characteristic derived from the dissipative equation of motion (1) balancing the effect of the driving force  $F_L(j)$  and the pinning-force density  $F_{\text{pin}}(v, T)$ . The right-most blue line represents the  $T = 0$  excess-current characteristic with a constant pinning force density  $F_{\text{pin}}(v, T) = F_c$ . The creep characteristics (red) are shown for temperatures  $T/e_p = (0.1, 0.5, 1, 1.5, 2.0) \times 10^{-2}$ , with the left-most curve corresponding to the highest temperature. The pinning-force densities for  $T > 0$  are calculated numerically (solid lines) and the resulting characteristics show good agreement with the analytic results (dashed, see Eq. (38)) in the regime of high and intermediate velocities  $v > v_{\text{TAFf}}$ . At low drives and low velocities (logarithmic plot in the inset), the characteristics exhibit the linear dependence on the drive  $j/j_c$  as described by Eq. (44); solid and dotted lines refer to numerical and analytic results, respectively.

characteristic in Fig. 5. The analytic predictions introduced above and further elaborated in sections III B and III C are in good agreement with the numerical results: While Eq. (38) describes the characteristic for high and intermediate velocities  $v > v_{\text{TAFf}}$ , the linear response formula Eq. (44) (including an accurate prefactor) gives a precise result at low drives (see inset of Fig. 5).

## B. Large drives, high velocities

In this section, we carry out the above program, that provides us with the modification of the excess-current characteristic at large drives due to thermal fluctuations, in particular, the thermal depinning current density  $j_{\text{dp}}(T)$  and the barrier  $U(j)$  determining the shape of the characteristic in the vicinity of  $j_{\text{dp}}(T)$ .

### 1. Energy landscape

We first find the boundaries  $x_{\pm}$  of the bistable region where second minima appear and disappear at  $r_{\pm}$ . The equilibrium condition (15),  $\partial_r e_{\text{pin}}(x_{\pm}; r)|_{r=r_{\pm}} = 0$ , then has to be simultaneously satisfied with the condition for an inflection point  $\partial_r^2 e_{\text{pin}}(x_{\pm}; r)|_{r=r_{\pm}} = 0$ , see Fig. 2. The combination of these two equations determines the end

points  $x_{\pm}$  of the multivalued interval together with the associated tip positions  $r_{\pm}$  at pinning and depinning,

$$f'_p(r_{\pm}) = \bar{C}, \quad x_{\pm} = r_{\pm} - \frac{f_p(r_{\pm})}{\bar{C}}. \quad (46)$$

Note that the inflection points  $r_{\pm}$  do not depend on the asymptotic vortex position  $x$  but are a property of the pinning potential in relation to the effective elasticity. Expanding the second equation away from  $x_-$  with  $x = x_- + \delta x_-$ , we find the tip locations of the free and unstable solutions near the onset of bistability,  $r_f(x) = r_- + \delta r$  and  $r_{us}(x) = r_- - \delta r$  with  $\delta r = (\xi \delta x_- / \kappa_-)^{1/2}$  and  $\kappa_- = \xi |f''_p(r_-)| / 2\bar{C}$ . Similarly, the tip locations of the pinned and unstable solutions at  $x = x_+ - \delta x$  close to  $x_+$  are given by  $r_p(x) = r_+ + \delta r$  and  $r_{us}(x) = r_+ - \delta r$  with  $\delta r = (\xi \delta x_+ / \kappa_+)^{1/2}$  and  $\kappa_+ = \xi f''_p(r_+) / 2\bar{C}$ . Simple estimates for  $\kappa_{\pm}$  are (see Appendix A)

$$\kappa_{\pm} = \frac{\xi |f''_p(r_{\pm})|}{2\bar{C}} \sim \sqrt{\kappa - 1} \quad (47)$$

at marginally strong pinning (we use that  $|f''_p(r_{\pm})| \sim (f_p/\xi^2)(\kappa - 1)^{1/2}$  and  $f_p/\bar{C}\xi \sim \mathcal{O}(1)$ ) and (see Appendix B)

$$\kappa_- \sim \kappa^{-1/(n+2)}, \quad \kappa_+ \sim \kappa \quad (48)$$

at very strong pinning (we use that  $f''_p(r_+) \sim f_p/\xi^2$ ,  $f_p/\bar{C}\xi \sim \kappa$ , and  $f''_p(r_-) \sim f_p/\kappa^{\nu}\xi^2$  with  $\nu = (n+3)/(n+2)$ )).

Next, we discuss the frequencies  $\omega_{p,f}$  and barriers  $U_{dp,p}$  in the rate equation (31). The deformation  $u$  of the vortex tip extends a distance  $z_{\text{tip}}$  of order the lattice constant  $a_0$  along the  $z$  direction. Given the viscosity  $\eta_l = \eta a_0^2$  for the motion of an individual vortex line, we approximate the tip motion by the dissipative dynamics of a particle with a friction coefficient  $\eta_l z_{\text{tip}} = \eta a_0^3$  in the effective potential  $e_{\text{pin}}(x; r = x + u)$ ,  $\eta a_0^3 \dot{u} = -\partial_u e_{\text{pin}}(x; x + u)$ ; the attempt frequencies then are given by the expressions<sup>32</sup>

$$\omega_p(x) = \frac{\sqrt{\lambda_p |\lambda_{us}|}}{2\pi \eta a_0^3}, \quad \omega_f(x) = \frac{\sqrt{\lambda_f |\lambda_{us}|}}{2\pi \eta a_0^3}, \quad (49)$$

where the curvatures  $\lambda_i$ ,  $i = p, f, us$ , are to be evaluated at the local minima and at the maximum of the pinning energy  $e_{\text{pin}}(x; r)$ ,

$$\lambda_i(x) = \partial_r^2 e_{\text{pin}}(x; r) \Big|_{r=r_i(x)} = \bar{C} - f'_p[r_i(x)]. \quad (50)$$

Since the curvatures  $\partial_r^2 e_{\text{pin}}(x; r)$  vanish at the inflection points  $r_i(x_{\pm})$ , we have  $\lambda_{p,us}(x_+) = \lambda_{f,us}(x_-) = 0$ . Close to the boundaries of the bistable regime, we obtain the expansions

$$\begin{aligned} \lambda_{f,us}(x_- + \delta x_-) &= \pm 2\bar{C}(\kappa_- \delta x_- / \xi)^{1/2}, \\ \lambda_{p,us}(x_+ - \delta x_+) &= \pm 2\bar{C}(\kappa_+ \delta x_+ / \xi)^{1/2}. \end{aligned} \quad (51)$$

Here, the  $\pm$  signs refer to the free/pinned and unstable branches. Simple estimates for the attempt frequencies then are (we remind that  $v_p = f_p/\eta a_0^3$  provides the velocity scale for dissipative motion in the pinning potential)

$$\omega_{p,f}(\delta x_{\pm}) \sim (v_p/\xi)(\kappa - 1)^{1/4} \sqrt{\delta x_{\pm}/\xi} \quad (52)$$

at marginally strong pinning and

$$\omega_p(\delta x_+) \sim (v_p/\xi) \sqrt{\delta x_+/\kappa \xi}, \quad (53)$$

$$\omega_f(\delta x_-) \sim (v_p/\xi) \kappa^{-\nu/2} \sqrt{\delta x_-/\kappa \xi} \quad (54)$$

at very strong pinning (we remind that  $\nu = (n+3)/(n+2)$ )).

Similarly, one finds for the onset of the barriers  $U_p(x) = e_{\text{pin}}(x; r_{us}(x)) - e_{\text{pin}}(x; r_f(x))$  and  $U_{dp}(x)$

$$U_p(x_- + \delta x_-) = \frac{4\bar{C}\xi^2}{3\sqrt{\kappa_-}} (\delta x_- / \xi)^{3/2}, \quad (55)$$

$$U_{dp}(x_+ - \delta x_+) = \frac{4\bar{C}\xi^2}{3\sqrt{\kappa_+}} (\delta x_+ / \xi)^{3/2}. \quad (56)$$

For marginally strong pinning, the interval of bistability shrinks as  $\propto (\kappa - 1)^{3/2}\xi$ , see Eq. (17), and the combination with the factor  $1/\sqrt{\kappa_{\pm}}$  produces barriers of size

$$U_{dp,p} \sim e_p(\kappa - 1)^2 \quad (57)$$

(note that  $\bar{C}\xi^2 \sim e_p/\kappa$ ). For very strong pinning, we find the bistability extending over the region  $x_+ - x_- \sim \kappa\xi$ . For the depinning and pinning barriers, we obtain

$$U_p \sim e_p \kappa^{\nu/2} (\delta x_- / \kappa \xi)^{3/2}, \quad U_{dp} \sim e_p (\delta x_+ / \kappa \xi)^{3/2}. \quad (58)$$

The expansions (51)–(56) break down for  $x$  close to the branch crossing point at  $x_0$ . However, one can still show that the depinning barrier  $U_{dp}$  decreases monotonically in the interval  $[x_-, x_+]$ . Indeed,  $U'_{dp}(x) = f'_{\text{pin}}(x) - f'_{\text{pin}}(x) = \bar{C}(r_p - r_{us}) < 0$ , see Fig. 2. The same way one shows that the pinning barrier  $U_p$  is monotonically increasing.

## 2. Solution of the rate equation

The first-order differential rate equation (31) for the occupation probability  $p(x)$  gives rise to two initial-value problems, to be solved separately in the multivalued intervals  $[-x_+, -x_-]$  and  $[x_-, x_+]$ . Within the first interval, the initial condition is  $p(-x_+) = 0$  (as the pinned branch only starts at  $-x_+$ ), while for the second,  $p(x_-) = 1$  (as there is only a pinned branch just before reaching  $x_-$ ). Note that, in principle, the solution can be discontinuous at the right end-points  $-x_-$  and  $x_+$  of the bistable intervals. Indeed, this is the case for the  $T = 0$  critical state occupation  $p_c(x)$ .

Focusing on the interval  $[x_-, x_+]$ , we assume a free branch with an exponentially small occupation  $1 - p$  and



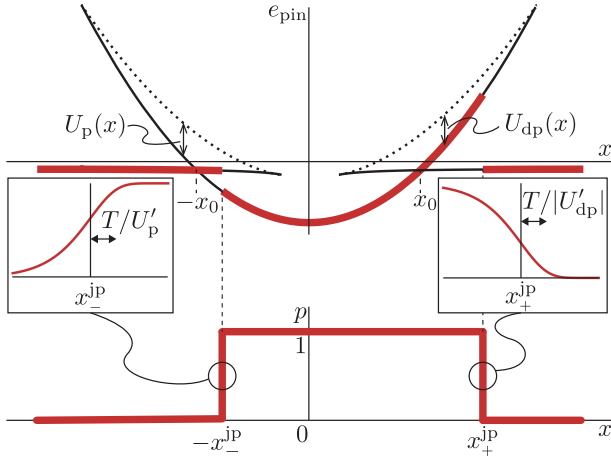


FIG. 6. Occupied branches (thick red) in the large velocity limit. The pinned-branch occupation  $p(x)$  is approximated by the top-hat function (bottom) with two jump points at  $-x_-^{\text{jp}}(v, T)$  and  $x_+^{\text{jp}}(v, T)$ . The insets show the variations of  $p(x)$  near the jump points occurring on scales  $T/|U'_p(-x_-^{\text{jp}})|$  and  $T/|U'_{\text{dp}}(x_+^{\text{jp}})|$  that are small compared to the spatial dimensions of the energy landscape.

neglect transitions from this branch as described by the second term on the right side of (31). The rate equation is then rewritten through the depinning relaxation length, see Eq. (34), as

$$\partial_x p = -p/\ell_{\text{dp}}(x). \quad (59)$$

We define the jump point  $x_+^{\text{jp}}$  through the condition  $\partial_x^2 p|_{x_+^{\text{jp}}} = 0$ , i.e., as the inflection point of  $p(x)$  or equivalently the point with the steepest rate of change of the occupation of the pinned branch. Taking the derivative of Eq. (59) with respect to  $x$ , we obtain the condition  $\partial_x^2 p(x) = [p/\ell_{\text{dp}}(x)^2][1 + \ell'_{\text{dp}}(x)]$  and the inflection point satisfies the relation  $\ell'_{\text{dp}}(x) = -1$ . Evaluating  $\ell'_{\text{dp}}(x)$  with the help of Eq. (34), we find that

$$\ell'_{\text{dp}}(x) = \left[ \frac{U'_{\text{dp}}(x)}{T} - \frac{\omega'_p(x)}{\omega_p(x)} \right] \ell_{\text{dp}}(x). \quad (60)$$

At small temperatures  $T \ll U_{\text{dp}}(x_+^{\text{jp}})$  the second term can be dropped and we obtain the condition for depinning in the form  $\ell_{\text{dp}}(x_+^{\text{jp}}) \approx T/|U'_{\text{dp}}(x_+^{\text{jp}})|$ . Finally, substituting back the definition Eq. (34) of  $\ell_{\text{dp}}$  provides us with the condition

$$v = \frac{\omega_p(x_+^{\text{jp}})T}{|U'_{\text{dp}}(x_+^{\text{jp}})|} \exp\left[-\frac{U_{\text{dp}}(x_+^{\text{jp}})}{T}\right]. \quad (61)$$

Eq. (61) is our quantitative condition determining the jump point  $x_+^{\text{jp}}(v, T)$  out of the pin, with the exponential providing the dominant factor. Since the barrier should be large as compared to the temperature  $T$  in order to validate Kramer's rate theory, the above results apply for

$x_+^{\text{jp}}$  not too close to  $x_+$ , i.e.,  $x_+ - x_+^{\text{jp}} \gg (T/e_p)^{2/3}\kappa\xi$  at strong pinning, see Eq. (58).

With increasing velocity  $v$ , the barrier  $U_{\text{dp}}$  decreases and the jump point approaches  $x_+$  where vortices depin without activation. The velocity  $v$  for activated motion then is restricted by the thermal velocity  $v_{\text{th}}$  that follows from Eq. (61) in the limit  $x_+^{\text{jp}} \rightarrow x_+$  where the barrier  $U_{\text{dp}}(x_+^{\text{jp}})$  vanishes. Using the expansions (51) and (56) for the barrier and the frequency factor  $\omega_p$  near the point  $x_+$ , we find

$$v_{\text{th}} = \lim_{x_+^{\text{jp}} \rightarrow x_+} \frac{\omega_p(x_+^{\text{jp}})T}{|U'_{\text{dp}}(x_+^{\text{jp}})|} = \frac{Tf_p''(r_+)}{4\pi C\eta a_0^3} \quad (62)$$

$$= \frac{\kappa_+}{2\pi} \frac{T}{\eta a_0^3 \xi} \sim \frac{T}{e_p} \kappa_+ v_p,$$

where  $v_p \sim f_p/\eta a_0^3$  is the velocity scale of dissipative motion in the well above which dynamical effects become relevant in the depinning process, see Ref. [11 and 12]. The thermal velocity  $v_{\text{th}}$  separates two regimes, the small velocity regime  $v < v_{\text{th}}$  where barriers are finite and creep is relevant, and the high velocity region where the occupation  $p(x)$  is given by the critical one,  $p(x) \approx p_c(x)$ , and the pinning-force density is approximately given by the critical value  $F_c$ , Eq. (27), as long as  $v \ll v_p$ . The results in Refs. [11, 12] describe the dynamical situation at high velocities of order  $v_p$  and beyond.

Finally, we can use the result for the thermal velocity  $v_{\text{th}}$  and rewrite the jump condition Eq. (61) in the form

$$U_{\text{dp}}(x_+^{\text{jp}}) \approx T \ln \frac{v_{\text{th}}}{v}. \quad (63)$$

As the velocity  $v$  decreases far below  $v_{\text{th}}$ , the quantity  $\omega_p T/|U'_{\text{dp}}|$  in Eq. (63) will deviate from its value at  $v_{\text{th}}$ , resulting in logarithmic corrections which we neglect in comparison with the large ratio  $U_{\text{dp}}(x_+^{\text{jp}})/T$ .

An analogous consideration applies to the interval  $[-x_+, -x_-]$  and provides us with the condition for the pinning barrier  $U_p(-x_-^{\text{jp}})$  determining the jump location  $-x_-^{\text{jp}} > -x_0$  where transitions from the free to the pinned branch start to become energetically favorable,

$$U_p(-x_-^{\text{jp}}) = T \ln \frac{v_{\text{th}}^-}{v}, \quad v_{\text{th}}^- = \frac{\kappa_-}{2\pi} \frac{T}{\eta a_0^3 \xi} \sim \frac{T}{e_p} \kappa_- v_p. \quad (64)$$

The ratio of velocity scales  $v_{\text{th}}^-/v_{\text{th}} = \kappa_-/\kappa_+$  is of order unity at marginally strong pinning and decays as  $\kappa^{-\nu}$  at very strong pinning. The activation barriers are thus approximately related by

$$U_p(-x_-^{\text{jp}}) \approx U_{\text{dp}}(x_+^{\text{jp}}) - \nu T \ln \kappa. \quad (65)$$

In the following, we neglect the small difference between the effective pinning and depinning barriers as both of them are supposed to be large compared to  $T$ . The conditions fixing the two jump points  $x_{\pm}^{\text{jp}}$  as a function of  $v$  and  $T$  then can be written in the simple form

$$U_{\text{dp}}(x_+^{\text{jp}}) \approx U_p(-x_-^{\text{jp}}) \approx U(v, T) \equiv T \ln \frac{v_{\text{th}}}{v}. \quad (66)$$

Next, we integrate Eq. (59) with the boundary condition  $p(x_-) = 1$  in order to find the full functional solution  $p(x)$  of the rate equation inside the interval  $[x_-, x_+]$ ,

$$p(x) = \exp \left[ -\frac{1}{v} \int_{x_-}^x dx' \omega_p(x') e^{-U_{dp}(x')/T} \right]. \quad (67)$$

The depinning barrier  $U_{dp}(x')$  decreases with  $x'$  such that at low temperatures the integral is dominated by its contributions close to the upper limit, while the lower limit  $x_-$  is irrelevant. The factor  $e^{-U_{dp}/T}$  entering the depinning distance  $\ell_{dp}$  changes on the scale  $T/|U'_{dp}|$ , while the change in the frequency  $\omega_p$  is negligible on this scale. Expanding  $U_{dp}(x')$  to linear order near the upper boundary  $x$  of the integral and neglecting variations of  $\omega_p(x')$  then gives

$$\begin{aligned} p(x) &\approx \exp \left[ -\frac{\omega_p(x)}{v} \int_{-\infty}^x dx' e^{-[U_{dp}(x) + U'_{dp}(x)(x' - x)]/T} \right] \\ &= \exp \left[ -\frac{\omega_p(x)T}{v|U'_{dp}(x)|} e^{-U_{dp}(x)/T} \right]. \end{aligned} \quad (68)$$

Expanding around the jump point  $x_+^{jp}$  as defined by the Eq. (61) and neglecting the changes of  $\omega_p(x)$  and  $|U'_{dp}(x)|$  on the scale  $T/|U'_{dp}(x_+^{jp})|$ , we find the expansion of  $p(x)$  near the jump point,

$$p(x_+^{jp} + \delta x) \approx \exp \left[ -e^{|U'_{dp}(x_+^{jp})|\delta x/T} \right]. \quad (69)$$

Indeed, the transition from  $p(x) = 1$  to  $p(x) = 0$  at  $x_+^{jp}$  is realized on a scale  $\ell_{dp}(x_+^{jp}) = T/|U'_{dp}(x_+^{jp})| \sim [T/e_p] \kappa \xi$ , that is small compared to the range  $\kappa \xi$  of the pinning landscape, see the inset of Fig. 6.

### 3. Pinning force

Given the thermally renormalized jumps at  $\pm x_{\pm}^{jp}$ , the average pinning force  $\langle f_{pin}(v, T) \rangle$  acting on vortices straightly impacting on a defect reads (see Eq. (23))

$$\langle f_{pin}(v, T) \rangle = \frac{\Delta e_{pin}^{tot}(v, T)}{a_0}, \quad (70)$$

with  $\Delta e_{pin}^{tot}(v, T) = \Delta e_{pin}(x_+^{jp}) - \Delta e_{pin}(-x_-^{jp}) > 0$ . Again, we have to generalize this result to the situation where vortices approach the defect at arbitrary transverse distance  $y$ . Assuming a radially symmetric defect potential, the same arguments can be made as for the  $T = 0$  situation, but with the jump from the free to the pinned branch now determined by the condition  $U_p(x, y) = U_p[(x^2 + y^2)^{1/2}, 0] = U(v, T)$ . The condition for vortex pinning thus becomes  $(x^2 + y^2)^{1/2} = x_{\pm}^{jp}$ , implying that vortices approaching the pin at a transverse distance  $y < t_{\perp} = x_{\pm}^{jp}$  get trapped (note that the transverse trapping length is enhanced compared to the  $T = 0$  case).

As a result, we find the finite-temperature pinning-force density to be given by

$$F_{pin}(v, T) = n_p \frac{2x_{\pm}^{jp}}{a_0} \frac{\Delta e_{pin}^{tot}(v, T)}{a_0}.$$

Below, we will make strong use of the scaled pinning-force density

$$\frac{F_{pin}(v, T)}{F_c} = \frac{x_{\pm}^{jp}(v, T)}{x_-} \frac{\Delta e_{pin}^{tot}(v, T)}{\Delta e_c} \quad (71)$$

that depends only on the rescaled barrier  $U(v, T)/e_p$ : indeed, the activation barrier  $U(v, T)$  suffices to determine the position of the jumps  $\pm x_{\pm}^{jp}$  as well as the magnitude of the jumps in energy. Let us analyze this force ratio as a function of velocity.

At marginally high velocities close to  $v_{TAF} = v_{th} e^{-U_0/T}$ , vortices probe barriers close to the maximum activation barrier  $U_0$  and the jumps  $x_{\pm}^{jp}$  in the energy landscape are realized close to the branch crossing point  $x_0$ . At velocities beyond  $v_{TAF}$ , the barriers and energy jumps scale linearly in the differences  $\delta x_0 = x_+^{jp} - x_0$  (and  $-x_-^{jp} + x_0$ ), resulting in a force ratio that is linear in the activation barrier  $U$  and that vanishes for  $U = U_0$ ,

$$\frac{F_{pin}(v, T)}{F_c} \approx \varphi(\kappa) \frac{U_0 - U(v, T)}{e_p} = \varphi(\kappa) \frac{T}{e_p} \ln \frac{v}{v_{TAF}}. \quad (72)$$

The exact expression for the slope  $\varphi(\kappa)$  is given in Appendix E. The function  $\varphi(\kappa)$  scales as  $\sim (\kappa - 1)^{-2}$  for marginally strong pinning  $\kappa \rightarrow 1$  and decays as  $\propto \kappa^{-\nu'}$  with the power  $\nu' = (3n + 4)/2(n + 1)(n + 2)$  at large  $\kappa$ , hence the function  $\tilde{\varphi}(\kappa) = \varphi(\kappa)(\kappa - 1)^2 \kappa^{\nu' - 2}$  is a slowly varying function in  $\kappa$  ranging between  $\tilde{\varphi}(\infty) \approx 3.1$  and  $\tilde{\varphi}(1) \approx 5.3$ , see Fig. 14.

At large velocities  $v \lesssim v_{th}$ , the departure from the critical force  $F_c$  is non-linear in  $(T/e_p) \ln(v/v_{th})$ , a result that is due to the non-linear scaling of the activation barrier with distance away from the critical jumps at  $x_{\pm}$ , see Eq. (55). Given the jumps at  $x_+^{jp} = x_+ - \delta x_+$  and  $x_-^{jp} = -x_- - \delta x_-$ , we expand the total jump in energy as given by Eq. (33) in the small quantities  $\delta x_+$  and  $\delta x_-$ ,

$$\Delta e_{pin}^{tot}(v, T) - \Delta e_c = \Delta f_{pin}(x_+) \delta x_+ - \Delta f_{pin}(-x_-) \delta x_-,$$

where  $\Delta f_{pin}(x_+) < 0$  and  $\Delta f_{pin}(-x_-) = -\Delta f_{pin}(x_-) > 0$ . The reduced jump in energy implies a reduction in  $\langle f_{pin}(v, T) \rangle$  as compared to its  $T = 0$  value. On the other hand, the trapping distance  $x_{\pm}^{jp}$  is larger by  $\delta x_{\pm}$  as compared to  $x_{\pm}$ , hence, more vortices are trapped at  $T > 0$ . These two effects compete as expressed in the expansion of the force ratio Eq. (71), to linear order,

$$\frac{F_{pin}}{F_c} \approx 1 + \frac{\delta x_-}{x_-} + \frac{\Delta f_{pin}(x_+) \delta x_+ + \Delta f_{pin}(x_-) \delta x_-}{\Delta e_c}, \quad (73)$$

where the first correction arises from the relative change in the trapping distance  $t_{\perp}$ , see Fig. 4, while the second correction is the relative change in the pinning force exerted on the vortex.

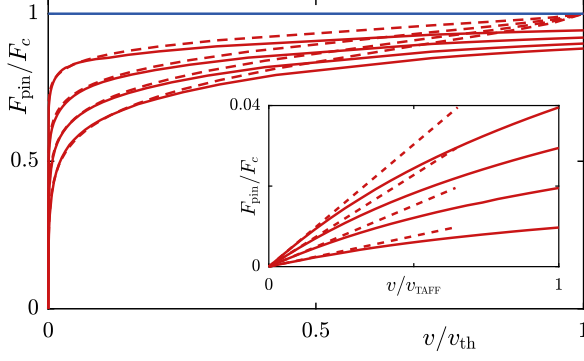


FIG. 7. Pinning-force density  $F_{\text{pin}}(v, T)$  calculated for the Lorentzian pinning potential and a Labusch parameter  $\kappa = 5$  at temperatures  $T/e_p = (0, 0.5, 1, 1.5, 2.0) \times 10^{-2}$  (top to bottom, solid blue line corresponds to  $T = 0$ ). The numerical result (solid line) as obtained from integrating Eq. (45) is compared with the analytical formula (dashed line) for high velocities, Eq. (75), and low velocities (inset, Eq. (124)). The pinning-force density is reduced compared to the critical force density  $F_c$  due to thermal creep at velocities  $v < v_{\text{th}}$ . While numerical and analytic results agree qualitatively, they differ quantitatively close to  $v_{\text{th}}$ . The inset shows the crossover to the linear TAFF response relevant for small velocities  $v < v_{\text{TAFF}}$ ; here the highest temperature corresponds to the uppermost curve, case  $T = 0$  is not shown.

We use Eqs. (55)–(56) to express  $\delta x_{\pm}$  through the activation barrier  $U(v, T)$ ,  $\delta x_{\pm} = \xi(3U\sqrt{\kappa_{\pm}}/4\bar{C}\xi^2)^{2/3}$ , and arrive at the expansion

$$\frac{F_{\text{pin}}(v, T)}{F_c} \approx 1 - g(\kappa)[U(v, T)/e_p]^{2/3} \quad (74)$$

$$= 1 - g(\kappa)\left(\frac{T}{e_p} \ln \frac{v_{\text{th}}}{v}\right)^{2/3}, \quad (75)$$

with the coefficient

$$g(\kappa) = -\frac{\xi \bar{\kappa}_-}{x_-} + \frac{\xi}{\Delta e_c} |\Delta f_{\text{pin}}(x_+) \bar{\kappa}_+ + \Delta f_{\text{pin}}(x_-) \bar{\kappa}_-|, \quad (76)$$

where  $\bar{\kappa}_{\pm} = [3e_p\sqrt{\kappa_{\pm}}/4\bar{C}\xi^2]^{2/3}$ ; this factor is of order  $\sim (\kappa - 1)^{1/6}$  for marginally strong pinning and  $\bar{\kappa}_+ \sim \kappa$ ,  $\bar{\kappa}_- \sim \kappa^{(2n+3)/3(n+2)}$  for very strong pinning.

The second term  $\propto \xi/\Delta e_c$  in Eq. (76) is always positive and dominates at marginally strong pinning, where  $|\Delta f_{\text{pin}}(x_{\pm})| \sim (e_p/\xi)(\kappa - 1)^{1/2}$  and  $\Delta e_c \sim (\kappa - 1)^2 e_p$ , hence  $g_+(\kappa) \sim (\kappa - 1)^{-4/3}$ , see Appendix E. The pinning force density  $F_{\text{pin}}(v, T)$  then is reduced compared to the critical force density  $F_c$  for sufficiently small  $\kappa$ . For very strong pinning, the second term is of order  $\kappa^0$ , hence the function  $\tilde{g}(\kappa) = g(\kappa)(\kappa - 1)^{4/3}\kappa^{-4/3} \approx 3.6$  is slowly varying in this regime, see Fig. 14. On the other hand, at ultra-strong pinning, the first term originating from the enhanced trapping distance is of order  $\sim -\kappa^{2n/3(n+2)}$  and eventually dominates over the positive second term,

see Appendix B. The function  $g(\kappa)$  then turns negative for  $\kappa > \kappa_0$  and grows in magnitude with a power of  $\kappa$ , implying a creep-enhanced pinning-force density beyond  $F_c$ ,  $F_{\text{pin}} > F_c$ , see Eq. (74). However, the crossover value  $\kappa_0$  where  $g$  turns negative is large and hardly accessible in a real material: for a Lorentzian potential, we find that  $\kappa_0 \approx 150$ , while for the exponentially decaying pinning potential  $e_p(r) = e_p/\cosh(r/\xi)$ , the crossover value is reduced but still large,  $\kappa_0 \approx 37$ .

In Fig. 7, we compare the numerical results derived from integrating Eq. (45) for the pinning-force density with those obtained from the analytic expression Eq. (75). The analytic solution predicts a somewhat larger pinning-force density at large velocities  $v \sim v_{\text{th}}$ . This enhancement originates from assuming sharp jumps in the branch occupation  $p(x)$  at the points  $\pm x_{\pm}^{\text{jp}}$  that is no longer valid at large velocities  $v \sim v_{\text{th}}$ : indeed for the depinning point, we have  $x_+^{\text{jp}} \rightarrow x_+$  for  $v \rightarrow v_{\text{th}}$  and the width  $T/|U'_{\text{dp}}(x_+^{\text{jp}})| \propto (x_+ - x_+^{\text{jp}})^{-1/2}$  of the jump in Eq. (69) diverges. In contrast to the analytic solution assuming a fully occupied pinned branch up to  $x_+$ , the regions of the pinned branch close to  $x_+$  responsible for large pinning forces become only partially occupied. The numerical solution taking into account this partial occupation then predicts a smaller pinning force.

Neither the analytic nor the numerical result is expected to be quantitatively accurate for  $v \sim v_{\text{th}}$ , as the assumption of large activation barriers  $U \gg T$  required by Kramer's rate theory is no longer satisfied. Nevertheless, in the wide and important region of intermediate velocities  $v_{\text{TAFF}} \ll v \ll v_{\text{th}}$  where barriers are large, both analytical and numerical results are reliable and show good agreement. As the velocity decreases, the pinning-force density (75) valid at large drives where barriers scale  $\propto \delta x_+^{3/2}$  has to be replaced by (72) (where barriers scale linearly in  $\delta x_0$ ); at very small velocities  $v < v_{\text{TAFF}}$ , the barrier saturates at  $x_0$  and we enter the linear response regime discussed in Sect. III C.

#### 4. Current-velocity characteristic

Applying the equation of motion (1) and the results for the force density ratio  $F_{\text{pin}}/F_c$  provides us with the current-velocity characteristic of the superconductor. We first consider velocities,  $v_{\text{TAFF}} \ll v < v_{\text{th}}$  where the expression (75) for the pinning force ratio holds and assume a regular situation with  $g(\kappa) > 0$ , see Sec. III C for a discussion of small velocities  $v \ll v_{\text{TAFF}}$ . Then the scaled equation of motion, to be solved for the velocity  $v$  at given drive  $j$ , takes the form

$$\frac{v}{v_c} = \frac{j}{j_c} - 1 + g(\kappa) \left[ \frac{T}{e_p} \ln \frac{v_{\text{th}}}{v} \right]^{2/3}. \quad (77)$$

This expression is conveniently rewritten into the form

$$\frac{v}{v_{\text{th}}} = \frac{1}{\mathcal{A}} \frac{\delta j}{j_c} + \frac{1}{\nu} \left[ \ln \left( \frac{v_{\text{th}}}{v} \right) \right]^{2/3} \quad (78)$$

with  $\delta j = j - j_c$ ,  $\mathcal{A}$  the ratio of thermal- and free-flow velocities

$$\mathcal{A} \equiv \frac{v_{\text{th}}}{v_c} = \frac{\kappa_+}{2\pi} \frac{T}{F_c a_0^2 \xi} = \frac{\kappa_+}{4\pi} \frac{T}{\Delta e_c} \frac{1}{n_p a_0 x_- \xi} \quad (79)$$

$$= \frac{T}{e_p} \frac{a(\kappa)}{n_p a_0 \xi^2} \quad (80)$$

involving the  $\kappa$ -dependent scaling factor

$$a(\kappa) = \frac{\kappa_+}{4\pi} \frac{\xi}{x_-} \frac{e_p}{\Delta e_c} \sim \begin{cases} \kappa^{-1/(n+2)}, & 1 \ll \kappa, \\ (\kappa - 1)^{-3/2}, & 1 \lesssim \kappa. \end{cases} \quad (81)$$

and the parameter

$$\nu = \frac{\mathcal{A}}{g(\kappa)} \left( \frac{e_p}{T} \right)^{2/3} = \left( \frac{T}{e_p} \right)^{1/3} \frac{a(\kappa)}{n_p a_0 \xi^2 g(\kappa)}. \quad (82)$$

Given the above asymptotic behavior, the function  $\tilde{a}(\kappa) = a(\kappa)(\kappa - 1)^{3/2} \kappa^{-(3n+4)/(2n+4)}$  is roughly constant and ranges between  $\tilde{a}(1) \approx 0.092$  and  $\tilde{a}(\infty) \approx 0.22$ , see Fig. 14 in Appendix E. The divergences in  $\mathcal{A} \propto (\kappa - 1)^{-3/2}$  and in  $\nu \propto (\kappa - 1)^{-1/6}$  as  $\kappa \rightarrow 1$  are due to the vanishing of the multi-stable solutions, in particular, the stabilizing barriers separating free and pinned branches. At the same time, the condition for the activation barriers being large compared to the temperature requires  $T \ll e_p(\kappa - 1)^2$  at marginally strong pinning. This compensates the divergences in  $\mathcal{A}$  and  $\nu$  and implies that the quantities  $(T/e_p)a(\kappa)$  and  $(T/e_p)^{1/3}a(\kappa)/g(\kappa)$  are small parameters. They compete with another small quantity  $n_p a_0 \xi^2$  (the 3D bulk strong pinning regime requires  $\kappa n_p a_0 \xi^2 < 1$ ) and so the parameters  $\mathcal{A}$  and  $\nu$  can assume both large and small values; we discuss below the possible scenarios.

In a first characterization of thermal effects, we determine the velocity ratio  $v(j_c)/v_{\text{th}}$  at the critical drive; with the finite  $T$  and  $T = 0$  characteristics joining at  $v_{\text{th}}$ , this quantity tells us about the importance of thermal fluctuations.

At moderately low temperatures such that  $1 \gg T/e_p \gg n_p a_0 \xi^2/a(\kappa)$ , we have  $\mathcal{A} \gg 1$  and therefore  $v_{\text{th}} \gg v_c$ , i.e., the characteristic joins the  $T = 0$  excess current characteristic at the current  $(1 + \mathcal{A})j_c$  far above  $j_c$ . Since  $\nu/\mathcal{A} = (e_p/T)^{2/3}/g(\kappa) \sim [(\kappa - 1)^2 e_p/T]^{2/3} \gg 1$ , this implies  $\nu \gg 1$  as well. We derive  $v(j_c)$  from Eq. (78) using the iterative scheme

$$\begin{aligned} \frac{v^{(0)}(j_c)}{v_{\text{th}}} &= \frac{1}{\nu}, \\ \frac{v^{(n+1)}(j_c)}{v_{\text{th}}} &= \frac{1}{\nu} \left[ \ln \frac{v_{\text{th}}}{v^{(n)}(j_c)} \right]^{2/3}. \end{aligned} \quad (83)$$

The velocity at critical drive can be formally expressed as  $v(j_c) = \lim_{n \rightarrow \infty} v^{(n)}(j_c)$ . In the following, we will always ignore corrections beyond  $\ln[\ln(\dots)]$  terms. For the velocity at critical drive  $j_c$ , we approximate

$$\frac{v(j_c)}{v_{\text{th}}} \approx \frac{1}{\nu} \left[ \ln \frac{\nu}{(\ln \nu)^{2/3}} \right]^{2/3}. \quad (84)$$

At very low temperatures, we enter the regime  $\mathcal{A} \ll 1$  and hence  $v_{\text{th}} \ll v_c$ . The characteristic joins the  $T = 0$  excess-current characteristic only slightly above  $j_c$  but the velocity  $v(j_c)$  may scale according to two different scenarios: If  $\nu \gg 1$ , i.e.,  $a(\kappa)n_p a_0 \xi^2 \gg T/e_p \gg [g(\kappa)/a(\kappa)]^3 (n_p a_0 \xi^2)^3$ , the iteration (83) can be applied and  $v(j_c)$  is appreciably suppressed (by  $\sim 1/\nu$ ) as compared to  $v_{\text{th}}$ . If the temperature is extremely low,  $T/e_p \ll [g(\kappa)/a(\kappa)]^3 (n_p a_0 \xi^2)^3$ , we eventually have  $\nu \ll 1$  and the iteration procedure can no longer be used (the convergence criterion is  $\nu > (2e/3)^{2/3} \simeq 1.49$ , see Appendix D). For those small values of  $\nu$ , we use the expansion  $v(j_c) = v_{\text{th}} - \delta v$  with  $\delta v \ll v_{\text{th}}$  in Eq. (78), what yields the correction  $\delta v/v_{\text{th}} \approx \nu^{3/2}$  and thus

$$\frac{v(j_c)}{v_{\text{th}}} \approx 1 - \nu^{3/2}, \quad \nu \ll 1, \quad (85)$$

i.e.,  $v(j_c)$  is very close to  $v_{\text{th}}$ .

Next, we use the ratio  $v(j_c)/v_c$  to define a depinning temperature  $T_{\text{dp}}$  where thermal fluctuations lead to a substantial change in the characteristic. Substituting the (*ad hoc*) criterion  $[v(j_c)/v_c]_{T_{\text{dp}}} \equiv 1/2$  to Eq. (78) provides us with the relation

$$\frac{1}{2} = g(\kappa) \left[ \frac{T_{\text{dp}}}{e_p} \ln \frac{2a(\kappa)T_{\text{dp}}}{n_p a_0 \xi^2 e_p} \right]^{2/3} \quad (86)$$

which we solve iteratively for  $T_{\text{dp}}$ ,

$$\begin{aligned} \frac{T_{\text{dp}}}{e_p} &\approx \frac{1}{[2g(\kappa)]^{3/2} \ln(\gamma/\ln \gamma)}, \\ \gamma &= \frac{a(\kappa)/\sqrt{2}}{g^{3/2}(\kappa) n_p a_0 \xi^2} \gg 1. \end{aligned} \quad (87)$$

The depinning temperature  $T_{\text{dp}}$  vanishes as  $(\kappa - 1)^2$  when approaching the Labusch point and scales as  $T_{\text{dp}} \sim e_p$  for very strong pinning.

Effects of thermal fluctuations are also conveniently described through the differential resistivity  $\rho$  rescaled by the flux-flow resistivity  $\rho_{\text{ff}}$ . Differentiating Eq. (78), we find that

$$\frac{\rho}{\rho_{\text{ff}}} = \left[ \frac{\partial(j/j_c)}{\partial(v/v_c)} \right]^{-1} = \left[ 1 + \frac{2}{3\nu} \frac{v_{\text{th}}/v}{(\ln v_{\text{th}}/v)^{1/3}} \right]^{-1}. \quad (88)$$

As illustrated in Fig. 8, the differential resistivity assumes a step-like form that is smeared and shifted to lower current densities as  $T$  increases. We define the depinning current density  $j_{\text{dp}}(T)$  as the inflection point of  $\rho(j)$ , i.e., the point of the fastest rate of change of the differential resistivity. Solving the condition  $\partial^2 \rho / \partial j^2 = \partial^3 v / \partial j^3 = 0$  for  $v$  leads to the definition of depinning velocity  $v_{\text{dp}}$  (see Appendix D for details),

$$\frac{v_{\text{dp}}}{v_{\text{th}}} \approx \frac{1}{3\nu} \frac{1}{(\ln[3\nu(\ln 3\nu)^{1/3}])^{1/3}}. \quad (89)$$

The corresponding depinning current density  $j_{\text{dp}}(T)$ , where the characteristic rises steeply (and thus assumes

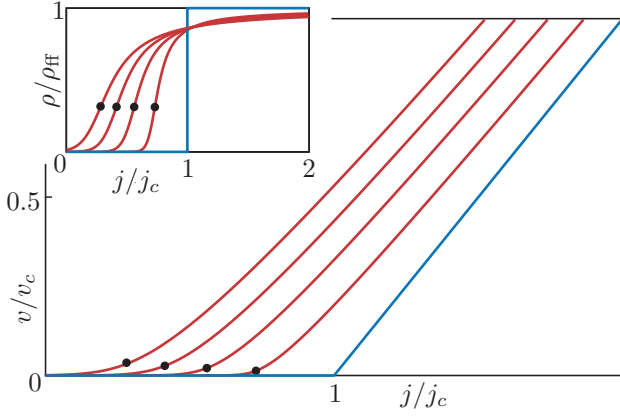


FIG. 8. Current-velocity characteristics at temperatures  $T/e_p = (0.50, 1.0, 1.5, 2.0) \times 10^{-2}$  and for a small defect density  $n_p a_0 \xi^2 = 10^{-4}$ . We have chosen the Labusch parameter  $\kappa = 5$  implying  $g(\kappa) \approx 2.8$  and  $a(\kappa) \approx 0.17$  for the Lorentzian pinning potential, which gives  $\mathcal{A} \approx 8.5$  for the lowest and  $\approx 34$  for the highest chosen temperature, respectively, guaranteeing the applicability of Kramer's rate theory for the range of velocities shown. The ratio of the chosen temperatures to the depinning temperature  $T_{dp} \approx 2.0 \times 10^{-2} e_p$  is  $T/T_{dp} = 0.25, 0.50, 0.75, 1.0$ . Thermal fluctuations lead to a downward shift of the critical current density  $j_c$  to the depinning current density  $j_{dp}(T)$  (solid points) defined through the inflection point in the differential resistivity (inset) where  $\rho(j_{dp}) \approx \rho_H/3$ . The characteristic steeply increases and follows roughly parallel to the excess-current characteristic past  $j_{dp}$ . The resistivity  $\rho$  steeply increases towards the flux-flow resistivity  $\rho_H$  around the depinning current  $j_{dp}$ ; the increase spreads around a wider region for higher temperatures.

the role of the  $T = 0$  critical current density  $j_c$ ), is conveniently written as a reduction of  $j_c$ ,  $\delta j_{dp}(T) = j_{dp}(T) - j_c < 0$  and reads

$$\frac{\delta j_{dp}(T)}{j_c} \approx \frac{g(\kappa)(T/e_p)^{2/3}}{(\ln[3\nu(\ln 3\nu)^{1/3}])^{1/3}} \left( \frac{1}{3} - \ln[3\nu(\ln 3\nu)^{1/3}] \right). \quad (90)$$

For very large  $\nu$  (note that  $\nu \gtrsim 100$  for the range of temperatures chosen in Fig. 8) the expression for the depinning current simplifies to

$$\frac{j_{dp}(T)}{j_c} \approx 1 - g(\kappa) \left( \frac{T}{e_p} \right)^{2/3} (\ln 3\nu)^{2/3}. \quad (91)$$

Substituting  $v_{dp}$  as calculated to order  $(\ln 3\nu)^{-4/3}$  to Eq. (88) (see Appendix D), we find that the differential resistivity at depinning remains approximately constant, with only a weak logarithmic temperature-dependence,  $\rho(j_{dp})/\rho_H \approx (1/3)[1 - (3 \ln 3\nu)^{-1}]$ .

Figure 8 shows both the current-velocity characteristic and the differential resistivity in the range of velocities  $v < v_c$ . Our main finding is the preservation of an excess-current characteristic also at finite temperatures, demonstrating that pinning and creep both remain active beyond  $j_c$ . Note the sharp rise of the characteristic

at  $j_{dp}(T)$  (replacing  $j_c$  at finite  $T$ ) and the nearly parallel shift of the flux-flow branch at large drives. To have Kramer's rate theory valid throughout the chosen range, we require that  $U(v_c, T) = T \ln \mathcal{A} \gtrsim T$ , which provides us with the condition  $\mathcal{A} \gg 1$ . Furthermore, in applying Kramer's rate theory, we have assumed that vortices reside in a local equilibrium state at any time during their motion. This is true for velocities  $v$  that are small compared to the scale  $v_p$  defined by the vortex dynamics during depinning,  $v_p \sim f_p/\eta a_0^3$ .

Indeed, for velocities beyond  $v_p$  the pinning force  $F_{pin}(v)$  decreases markedly, see Refs.<sup>11,12</sup>. The velocity scale  $v_p$  is independent on  $n_p$  and much larger than the flow velocity  $v_c$ ,  $v_c/v_p \sim n_p a_0 \xi^2 (\Delta e_c/f_p \xi)(x_-/\xi) \sim n_p a_0 \xi^2 (\kappa - 1)^2$  at moderate and  $\sim n_p a_0 \xi^2 \kappa^{(n+3)/(n+2)}$  for very strong pinning. This separation of scales guarantees the simple shape of the excess-current characteristic over a large regime  $v < v_p$  including the free-flow velocity  $v_c$  at  $F_c$ ; the inequality  $n_p a_0 \xi^2 \kappa < 1$  is the condition for 3D bulk strong pinning<sup>16</sup>. We then have to check that the thermal velocities  $v < v_{th}$  below which finite temperatures modify the excess-current characteristic remain below  $v_p$ . With (we drop numericals and logarithmic corrections)

$$\frac{v_{th}}{v_p} \sim \frac{T}{e_p} \kappa_+ \sim \frac{T}{T_{dp}} \frac{\kappa_+}{g(\kappa)^{3/2}}, \quad (92)$$

we find that this condition limits our temperature to a value below  $T_{dp}/\kappa$  at very strong pinning, else dynamical effects have to be accounted for. Note, however, that at temperatures  $\sim T_{dp}$  the characteristic has already lost the essential signatures of pinning, hence this limitation is easily satisfied. At marginally strong pinning, we have  $v_{th}/v_p \sim (\kappa - 1)^{5/2} (T/T_{dp})$  and the condition  $v_{th} < v_p$  is always satisfied for temperatures below  $T_{dp}$ .

## 5. Activation barriers

The creep-type motion of vortices leads to an average velocity  $v$  of the vortex lattice as discussed in the previous chapters. The pinning and depinning of individual vortices can be understood as a thermal diffusion process, with vortices undergoing transitions between the pinned and free metastable states. Hence, the activation barriers play a central role in determining the shape of the current-voltage characteristic. As explained in Secs. II and III, the barriers separating the pinned and free states depend on the distance  $x$  of the vortex from the nearest defect, with the transitions between states taking place close to the specific jump points  $\pm x_{\pm}^{jp}$ .

In order to obtain expressions for the activation barriers  $U(j)$  as a function of drive  $j$ , we use Eq. (66) to express  $U$  as function of temperature and velocity and then combine the result with the current-velocity characteristic  $v(j)$ , Eq. (77); the activation barrier  $U(j) = U(v(j), T)$  provides us with the characteristic in the Ar-



Arrhenius form  $v(j) = v_{\text{th}} e^{-U(j)/T}$  typical for a thermally activated motion.

A different behavior is expected for the creep barriers at small and large drives  $j$ : As the driving current  $j$  approaches  $j_c$  from below, the barrier is expected to vanish as<sup>1</sup>  $U(j) \approx U_c(1 - j/j_c)^\alpha$  with an exponent  $\alpha$  depending on the pinning scenario. For small currents  $j \rightarrow 0$ , the barriers are usually discussed in the context of weak pinning theory, predicting a glassy response of the vortex lattice with a diverging activation barrier  $U \approx U_0(j_0/j)^\mu$ .

Within the framework of strong pinning that assumes independent action of defects, the behavior of the activation barriers differs from this standard expectation. Starting at small drives  $j \rightarrow 0$ , the jump points  $x_\pm^{\text{JP}}$  approach the branch crossing point  $x_0$  with an activation barrier  $U_0 = U_p(x_0) = U_{\text{dp}}(x_0)$  that remains finite, hence glassy response is replaced by an ohmic one, see Sec. III C for details. For larger drives close to  $j_c$ , we discuss separately the two cases below and above vortex depinning. Sufficiently below  $j_c$ , the vortex velocity is small and the term  $v/v_c$  at the left of Eq. (77) can be neglected (this is equivalent to neglecting the dissipative forces acting on the vortex lattice). Using Eq. (66), we find the barrier

$$U(j) \approx U_c \left(1 - \frac{j}{j_c}\right)^{3/2}, \quad U_c = \frac{e_p}{g^{3/2}(\kappa)}. \quad (93)$$

This expression remains valid for currents not too close to  $j_c$ , as we can drop the term  $v/v_c$  only provided that  $v/v_c = \mathcal{A}e^{-U(j)/T} \ll 1 - j/j_c$ . As a result, Eq. (93) remains valid if

$$1 - \frac{j}{j_c} \gtrsim g(\kappa) \left(\frac{T}{e_p}\right)^{2/3} (\ln \nu)^{2/3}. \quad (94)$$

Dropping the numerical under the logarithm in Eq. (91), we can express this condition in the form  $j \lesssim j_{\text{dp}}(T)$ .

Beyond depinning, the vortex motion is characterized by a steep rise in velocity and the dissipative forces cannot be ignored any longer. The vortex motion is slowed down as compared to the pure thermally activated situation and the resulting barrier attains larger values than described by Eq. (93), see Fig. 9. In this regime, the current-velocity characteristic is approximately linear and joins the  $T = 0$  excess-current characteristic at a current  $(1 + \mathcal{A})j_c$  corresponding to the velocity  $v_{\text{th}}$ . The vortex velocity then can be approximated by

$$v(j) \approx v(j_c) + \frac{1}{\mathcal{A}}(j/j_c - 1)[v_{\text{th}} - v(j_c)]. \quad (95)$$

Using the expression for  $v(j_c)$  from Eq. (84), we find the barrier

$$U(j) \approx U(j_c) - T \ln \left[ 1 + \frac{1}{\mathcal{A}} \left( \frac{\nu}{(\ln \nu)^{2/3}} - 1 \right) \frac{j - j_c}{j_c} \right] \quad (96)$$

with the activation barrier at the critical drive  $U(j_c) \approx T \ln[\nu/(\ln \nu)^{2/3}]$ . Assuming  $\nu \gg 1$ , comparing with the

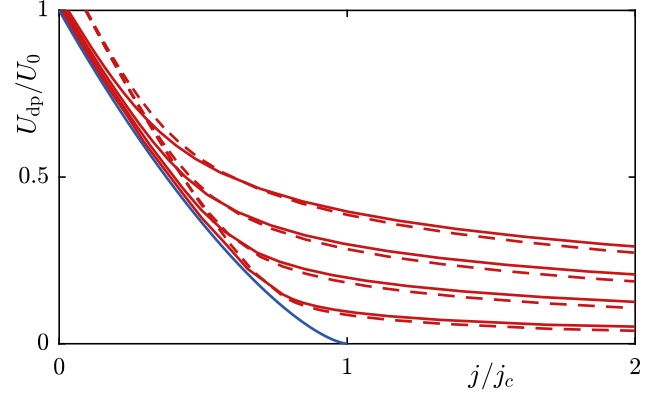


FIG. 9. Depinning barrier as function of the driving current at temperatures  $T/e_p = (0.5, 1.0, 1.5, 2.0) \times 10^{-2}$  and a small density of defects  $n_p a_0 \xi^2 = 10^{-4}$  for a Lorentzian pinning potential with  $\kappa = 5$ . The blue curve vanishing at  $j = j_c$  corresponds to the limit  $T \rightarrow 0$ , while higher temperatures produce non-vanishing barriers growing with temperature beyond  $j_c$ . The solid lines track the numerical results for the average barrier value, see Eq. (98). Dashed curves are the analytical approximation of the barriers as provided by Eqs. (93)–(97).

definition of the depinning current density, and ignoring numerical factors inside the logarithm, allows us to rewrite Eq. (96) as

$$U(j) \approx U(j_c) - T \ln \left[ 1 + \frac{j - j_c}{j_c - j_{\text{dp}}(T)} \right]. \quad (97)$$

As shown in Sect. III B 4, the effects of thermal depinning and creep persist well above the critical current  $j_c$ . In accordance with this result, the corresponding activation barrier vanishes at large currents  $j \sim (1 + \mathcal{A})j_c \gg j_c$ . The slow logarithmic decay of the barrier predicted by Eq. (97) then corresponds to the linear current-velocity characteristic.

In order to test the quality of our approximations, we compare the above analytical results with a computational scheme that relies on the numerical solution of the rate equation and the current-voltage characteristic. We exploit the insight that the transitions from pinned to free states go together with a smooth drop of the occupation probability  $p(x, y)$  from  $p = 1$  to  $p = 0$  when increasing  $x$  across the depinning jump point  $x_+^{\text{JP}}$ ; it is this region that defines the relevant barriers in the depinning process. The derivative  $\partial_x p$  is sharply peaked around  $x_+^{\text{JP}}$  and serves as a convenient measure (of total weight unity) to define the average depinning barrier,

$$\langle U_{\text{dp}} \rangle = \frac{1}{2x_-} \int_{-x_-}^{x_-} dy \int_{x_-}^{x_+} dx U_{\text{dp}}(x, y) [-\partial_x p(x, y)]. \quad (98)$$

The  $y$ -integration is cut by  $|y| = \pm x_-$  since vortices passing at larger transverse distances from the defect are not pinned. The average pinning barrier  $\langle U_p \rangle$  is defined in a similar way, with the  $x$ -integration ranging



from  $-x_+$  to  $-x_-$  and with the derivative replaced via  $-\partial_x p(x, y) \rightarrow \partial_x p(x, y)$  (during pinning, the branch occupation grows from  $p = 0$  to  $p = 1$ ). This scheme provides us with the average barrier at a particular temperature  $T$  and velocity  $v$  (since the solution of the rate equation is obtained at fixed  $T$  and  $v$ ); in order to obtain the activation barriers as function of drive  $j$ , we have to combine this result with the numerical predictions for the current-velocity characteristic. The result of this numerical procedure and its comparison with the analytical prediction are displayed on Fig. 9, with very satisfactory agreement between the two.

Against common expectations, our activation barrier grows with temperature in the region beyond depinning (cf. the expression for  $U(j_c)$  and Fig. 9). Thermal activation enhances the vortex motion and the magnitude of the pinning force  $F_{\text{pin}}(v, T)$  decreases with increasing temperature. Eq. (74) then relates the activation barrier  $U$  and the pinning-force density  $F_{\text{pin}}$  and shows that decreasing pinning forces indeed correspond to an increasing barrier. On a more technical level, within the strong pinning paradigm, the relevant barrier at a given drive  $j$  and temperature  $T$  is selected by the jump positions  $\pm x_{\pm}^{\text{jp}}$ ; increasing  $T$  pushes  $\pm x_{\pm}^{\text{jp}}$  further away from  $\pm x_{\pm}$  where the barriers are larger, see Figs. 3 and 6.

The current-dependence of the activation barrier  $U(j)$  is directly related to the magnetic relaxation rate<sup>1</sup> and, conversely, the measurement of creep rates can be used to reconstruct the barrier, a topic we are going to analyse in the next paragraph.

## 6. Magnetic relaxation through creep

Magnetic relaxation measurements<sup>36–38</sup> represent a convenient way to study thermal vortex creep. The sample is typically cooled in zero field, then a magnetic field is applied generating a Bean critical state with a vortex density gradient. Subsequently, this density gradient is relaxed as vortices move further into the sample due to creep, what results in a decay of the diamagnetic moment with time. The magnetization is linearly proportional to the persistent current  $j(t)$  flowing in the sample and the role of thermal fluctuations can be quantified via the creep rate  $S = -d \ln j / d \ln t$ , a quantity that is closely related to the activation barrier  $U(j)$ . Within the Anderson-Kim flux creep theory<sup>39</sup>, barriers are linear in the current, which results in the creep rate  $S = T/U_c$ . However, the observed creep rate often exhibits a finite value when extrapolated to small temperatures<sup>38</sup>, a feature that is usually ascribed to the phenomenon of quantum creep<sup>1,40</sup>. Below, we discuss creep rates in the framework of strong pinning theory with non-linear barriers near  $j_c$  and show that such a scenario may provide an alternative explanation of the apparent low- $T$  saturation phenomenon of creep.

Specifically, we consider a superconducting slab of thickness  $d$  in the presence of an external magnetic field.

Variations in the magnetic induction  $\mathbf{B}$  inside the slab lead to a transport current density  $\mathbf{j} = (c/4\pi)\nabla \times \mathbf{B}$ . The resulting Lorentz force density  $\mathbf{F}_L$  moves vortices in the direction of the gradient of  $\mathbf{B}$ , what diminishes the variation in the magnetic field and leads to the decay of the observed current density. Assuming activation barriers independent on the magnetic field, the time evolution of the current density  $j$  follows from

$$\frac{\partial j}{\partial t} = -\frac{j_c}{\tau_0} e^{-U(j)/T}, \quad (99)$$

where  $\tau_0$  denotes a macroscopic timescale, see Ref. [1] (we use Eqs. (66), (79) and  $\eta = BH_{c2}/c^2\rho_n$  in the second equation)

$$\tau_0 = \frac{\pi j_c d^2}{2c v_{\text{th}} H} = \frac{\pi}{2\mathcal{A}} \frac{H_{c2}}{H} \frac{d^2}{\rho_n c^2}. \quad (100)$$

Using typical values  $H/H_{c2} \sim 10^{-1}$ ,  $\rho_n \sim 10^{-4} \Omega \text{ cm}$ ,  $d \sim 0.1 \text{ cm}$ , we estimate the timescale  $\tau_0 \sim 10^{-5}/\mathcal{A}[s]$ , where the parameter  $\mathcal{A}$  depends on temperature  $T$ , density of defects  $n_p$ , and the Labusch parameter  $\kappa$  according to Eq. (79).

The differential equation (99) describing the creep induced decay of  $j(t)$  is easily transformed to one describing the evolution of the barrier  $U(t)$  and its integration produces the well known result<sup>1</sup>

$$U(t \gg t_0) \approx T \log(t/t_0), \quad (101)$$

with the new timescale defined self-consistently as  $t_0 = \tau_0 T / (j_c |\partial_j U|)$ . From Eq. (93), one finds that  $|\partial_j U| = (2/3)(U_c/j_c)(U/U_c)^{1/3}$ , that reduces the self-consistent relation to  $t_0 = (2\tau_0/3)(T/U_c)^{2/3}(\log t/t_0)^{1/3}$ . Ignoring logarithmic corrections, we obtain

$$t_0 = \frac{2}{3} \tau_0 g(\kappa) \left( \frac{T}{e_p} \right)^{2/3} = \frac{\pi}{3\nu} \frac{H_{c2}}{H} \frac{d^2}{\rho_n c^2} \sim \frac{10^{-5} \text{ s}}{\nu} \quad (102)$$

with  $\nu$  given in Eq. (82). Using a typical value  $\nu \sim 10^2$  then gives  $U(t = 10^3 \text{ s}) \approx 23 T$ , confirming the assumption  $U \gg T$ . The non-linear barrier (93) translates (101) into a slow time-decay of the screening current (or magnetization) that depends non-linearly on  $\log(t/t_0)$ ,

$$\frac{j(t)}{j_c} = 1 - \left( \frac{T}{U_c} \right)^{2/3} [\log(t/t_0)]^{2/3}. \quad (103)$$

Neglecting the temperature dependence of  $\log(t/t_0)$  (note that  $t_0$  depends on temperature through the parameter  $\nu$ ), we arrive at the expression for the normalized creep rate  $S = -d \log(j/j_c) / d \log(t/t_0)$ ,

$$S = \frac{2}{3} \frac{(T/U_c)^{2/3} [\log(t/t_0)]^{-1/3}}{1 - [(T/U_c) \log(t/t_0)]^{2/3}}. \quad (104)$$

This result predicts an initial non-linear and convex increase of the creep rate  $S \propto (T/U_c)^{2/3}$  at small temperatures, followed by a concave growth at higher

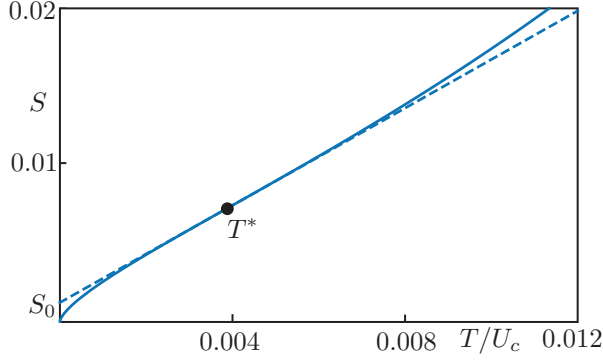


FIG. 10. Normalized creep rate  $S = -d \log(j/j_c)/d \log(t/t_0)$  as predicted by Eq. (104) for  $n_p a_0 \xi^2 = 10^{-3}$ ,  $\kappa = 5$  and a measurement time  $t = 10^3$  s. The initial non-linear increase  $S \propto (T/U_c)^{2/3}$  crosses over to the approximately linear regime near the inflection point  $T^*$  defined by  $\partial_T^2 S(T^*) = 0$ ,  $T^*/U_c = 1/[5^{3/2} \log(t/t_0)] \approx 4 \times 10^{-3}$ . Extrapolating the creep rate around the inflection point to zero temperatures yields a finite creep value  $S_0 \approx 1/[36 \log(t/t_0)] \approx 1.2 \times 10^{-3}$ .

temperatures beyond the inflection point at  $T^* = U_c/[5^{3/2} \log(t/t_0)]$ , see Fig. 10. Such a creep rate with a temperature dependence indicative for an inflection point has been observed in recent experiments<sup>38</sup>. As the limit  $T \rightarrow 0$  is not accessible, the extrapolation of such a line shape below  $T^*$  then reaches a finite value  $S_0 = S(T=0)$ ; a linear extrapolation at the inflection point  $T^*$  produces the result  $S_0 \approx 1/36 \log(t/t_0)$ . Such an extrapolation to a finite  $T=0$  creep rate within strong pinning theory then is in competition with the interpretation of a finite value  $S_0 > 0$  generated by quantum creep<sup>40</sup>.

Increasing the temperature beyond the inflection point  $T^*$ , the creep rate increases further and formally diverges when  $U_c = T \log(t/t_0)$ , see Eq. (104); under these conditions, the finite barriers have effectively vanished. In reality, this result is expected to be modified due to collective pinning effects appearing at small drive. Such collective effects will lead to diverging barriers and a saturation of the creep rate at fixed decay time  $t^1$ .

### C. Small drives, low velocities

As the velocity of the vortex system approaches values of order  $v_{\text{TAF}} \simeq v_{\text{th}} e^{-U_0/T}$ , the activation barrier  $U(v, T)$  reaches its maximum possible height  $U_0$  and the jump points  $x_{\pm}^{\text{jp}}$  approach the location  $x_0$  where the branches cross. The result Eq. (32) suggesting a vanishing pinning force (due to the vanishing energy jumps  $\Delta e_p(-x_0) = \Delta e_{\text{dp}}(x_0) = 0$ ) is no longer applicable. We then have to go back and solve the rate equation (31) for the present situation which involves both terms  $\propto p$  and  $\propto (1-p)$  in order to find the shape of  $p(x)$  near  $x_0$ .

We start from the equilibrium occupation  $p_{\text{eq}}(x)$  and

calculate the corrections due to a finite but weak drive  $j$  or small velocity  $v$ . Rewriting the rate equation (31) with the help of the equilibrium distribution (39), we can cast it into the form

$$\frac{dp}{dx} = (p_{\text{eq}} - p) \left( \omega_p e^{-U_{\text{dp}}/T} + \omega_f e^{-U_p/T} \right) \quad (105)$$

$$= \frac{p_{\text{eq}}(x) - p}{\ell_{\text{eq}}(x)}, \quad (106)$$

with the local equilibrium relaxation length

$$\ell_{\text{eq}}(x) = [\ell_p(x)^{-1} + \ell_{\text{dp}}(x)^{-1}]^{-1}. \quad (107)$$

#### 1. Equilibrium properties

In order to solve the rate Eq. (40), we need to analyze the equilibrium distribution  $p_{\text{eq}}(x)$  and relaxation length  $\ell_{\text{eq}}(x)$ . We restrict the discussion to the interval  $[x_-, x_+]$ ; a similar analysis applies to the region  $[-x_+, -x_-]$ . Using the definition of  $\ell_{\text{dp}}(x)$ , Eq. (34) (and analogous for  $\ell_p(x)$ ) and expressing the jump in energy  $\Delta e_{\text{pin}}$  through the difference of the barriers,  $\Delta e_{\text{pin}}(x) = U_p(x) - U_{\text{dp}}(x) > 0$ , we can rewrite the equilibrium distribution Eq. (39) in the form

$$p_{\text{eq}}(x) = \frac{1}{1 + (\omega_p/\omega_f) e^{\Delta e_{\text{pin}}/T}} \quad (108)$$

$$= \frac{1}{1 + (\lambda_p/\lambda_f)^{1/2} e^{\Delta e_{\text{pin}}/T}}. \quad (109)$$

The equilibrium distribution formulated through the Eq. (109) is expressed purely in terms of equilibrium properties of the energy landscape: the energy difference of branches  $\Delta e_{\text{pin}}$  and the curvatures  $\lambda_p, \lambda_f$  at the local minima of the double-well pinning energy  $e_{\text{pin}}(x; r)$ . The ratio of curvatures  $\lambda_p/\lambda_f$  plays an important role in the equilibrium probability distribution. The two minima, pinned and free, come with a different geometrical shape: e.g., at very strong pinning and  $x_- \ll x \ll x_+$ , we can estimate the curvatures (see Fig. 2)  $\lambda_p \sim e_p/\xi^2$  and  $\lambda_f \sim \bar{C}$ . As a result, the branches are not populated equally at the branch crossing point  $x_0$  where  $\Delta e_{\text{pin}}(x_0) = 0$ . For  $\kappa \gg 1$ , we find instead  $p_{\text{eq}}(x_0) \sim 1/\sqrt{\kappa}$ , i.e., the shallower well of the free branch is more strongly populated since it accommodates more states.

This implies that the point  $x_{\text{eo}}$  of equal branch occupation is shifted to the left from  $x_0$  (see Fig. 11 and the Appendix C for a more elaborate discussion). A similar analysis of the equilibrium relaxation length, Eq. (107), shows that the point  $x_{\text{lr}}$  where the relaxation length is maximal is also shifted to the left from  $x_0$  and that the three points,  $x_0, x_{\text{eo}}$ , and  $x_{\text{lr}}$  are arranged in the sequence  $x_{\text{eo}} < x_{\text{lr}} < x_0$ . For marginally strong pinning, the energy landscape becomes symmetric and the three positions join up.

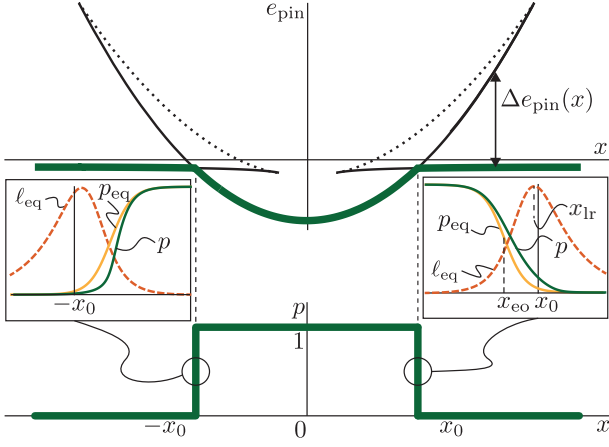


FIG. 11. Occupied branches (thick) of the multi-valued energy landscape for a Lorentzian pin with  $\kappa = 5$  in the low velocity limit  $v \ll v_{th} e^{-U_0/T}$ . The occupation changes sharply in the vicinity of the branch crossing points  $\pm x_0$  and  $p(x)$  takes the form of a shifted equilibrium occupation,  $p(x) \approx p_{eq}[x - \ell_{eq}(x)]$ ; the solid curves in the insets show the distribution functions  $p(x)$  and  $p_{eq}(x)$  near  $\pm x_0$  on an expanded scale. The dashed curves show the equilibrium relaxation distance  $\ell_{eq}(x)$  with the maxima attained at  $\pm x_{lr}$ ,  $x_{lr} \approx x_0 + [T/2(n+1)\Delta f_{pin}(x_0)] \ln \kappa$ . The points of equal equilibrium branch occupation are further shifted to  $\pm x_{eo}$ , with  $x_{eo} \approx x_0 + [T/2\Delta f_{pin}(x_0)] \ln \kappa$ .

## 2. Solution of the rate equation

We use the ansatz  $\delta p = p - p_{eq}$  in the rate equation (40) what takes us to the linear problem

$$\delta p' + \frac{\delta p}{\ell_{eq}(x)} = -p'_{eq} \quad (110)$$

with the boundary condition  $\delta p(x_-) = 0$ . The Green's function  $G(x, x')$  satisfying the differential equation

$$[\partial_x + \ell_{eq}(x)^{-1}]G(x, x') = \delta(x - x') \quad (111)$$

takes the form

$$G(x, x') = \Theta(x - x') \exp \left[ - \int_{x'}^x \frac{dx''}{\ell_{eq}(x'')} \right], \quad (112)$$

in terms of which the solution for (110) reads

$$\delta p(x) = - \int_{x_-}^x dx' G(x, x') p'_{eq}(x'). \quad (113)$$

Fixing  $x$  and varying  $x' < x$ , the function  $G(x, x')$  grows on a scale  $\ell_{eq}(x) \lesssim \ell_{eq}(x_{lr})$ , which is small compared to  $T/|U'_{dp}|$  or  $T/|U'_p|$ . As a result, the change in  $p'_{eq}(x)$  or  $\ell_{eq}(x)$  is small on this scale and we can approximate  $G(x, x') \approx e^{-(x-x')/\ell_{eq}(x)}$  as well as  $p'_{eq}(x') \approx p'_{eq}(x)$  in

Eq. (113). Moving the lower integration bound in Eq. (113) from  $x_-$  to  $-\infty$  provides us with the final result

$$\begin{aligned} p(x) &\approx p_{eq}(x) - \int_{-\infty}^x dx' \exp \left[ - \frac{x-x'}{\ell_{eq}(x)} \right] p'_{eq}(x) \\ &= p_{eq}(x) - \ell_{eq}(x) p'_{eq}(x) \approx p_{eq}[x - \ell_{eq}(x)]. \end{aligned} \quad (114)$$

Hence, we find that the branch occupation is shifted from its equilibrium distribution by a small distance  $\ell_{eq}(x)$ . This shift is small compared to the scale where the equilibrium distribution  $p_{eq}(x)$  changes.

## 3. Pinning force

The average pinning force  $\langle f_{pin} \rangle$  involves an integration over the asymptotic vortex positions  $x$ . Using the symmetry  $x \leftrightarrow -x$  of the integrand  $\ell_{eq} p'_{eq} \Delta f_{pin}$ , we can restrict the integration in Eq. (42) to the interval  $[x_-, x_+]$ ,

$$\langle f_{pin} \rangle = \frac{2}{a_0} \int_{x_-}^{x_+} dx \ell_{eq}(x) p'_{eq}(x) \Delta f_{pin}(x). \quad (115)$$

The functions  $p'_{eq}(x)$  and  $\ell_{eq}(x)$  are sharply peaked around  $x_{eo}$  and  $x_{lr}$  on the scale  $T/|\Delta f_{pin}|$ . We therefore expand  $\Delta e_{pin}(x_0 + \delta x) = -\Delta f_{pin} \delta x$  in Eq. (108) and neglect the  $x$ -dependence of the frequency factors  $\omega_{p,dp}$ . We find that

$$p'_{eq}(x_0 + \delta x) = \frac{\Delta f_{pin}/4T}{\cosh^2 \left[ \frac{-\Delta f_{pin}}{2T} \delta x + \frac{1}{2} \ln \frac{\omega_p}{\omega_f} \right]} \quad (116)$$

and similarly,

$$\ell_{eq}(x_0 + \delta x) = \frac{v e^{U_0/T}}{\sqrt{\omega_p \omega_f}} \frac{e^{(U'_p + U'_{dp}) \delta x / 2T}}{\cosh \left[ \frac{-\Delta f_{pin}}{2T} \delta x + \frac{1}{2} \ln \frac{\omega_p}{\omega_f} \right]}. \quad (117)$$

The limits of integration in Eq. (115) can be shifted to  $\pm\infty$  since the contributions from the region  $|\delta x| \gg T/|\Delta f_{pin}|$  are negligible. We abbreviate  $[(-\Delta f_{pin}/T) \delta x + \ln(\omega_p/\omega_f)]/2 = z$  and define the ratio

$$\Gamma = - \frac{U'_p + U'_{dp}}{\Delta f_{pin}} \Big|_{x_0} = \frac{U'_p + U'_{dp}}{U'_p - U'_{dp}} \Big|_{x_0} \quad (118)$$

ranging between  $\Gamma = 0$  for marginally strong pinning where  $U'_p \approx -U'_{dp}$  and  $\Gamma = 1$  for very strong pinning with  $U'_p \gg |U'_{dp}|$ . Furthermore, we ignore variations of  $\Delta f_{pin}$  that appear on the large scale  $\kappa \xi$ . With these approximations, the average pinning force is given by

$$\langle f_{pin} \rangle = \frac{v |\Delta f_{pin}| (\omega_p/\omega_f)^{-\Gamma/2} e^{U_0/T}}{2a_0 \sqrt{\omega_p \omega_f}} \int_{-\infty}^{\infty} dz \frac{e^{\Gamma z}}{\cosh^3 z}. \quad (119)$$

The integral can be evaluated by deforming the contour in the complex plane around the poles

$z_n = (n + \frac{1}{2})\pi i$ ,  $n \in \mathbb{Z}_0^+$ . The residues  $\text{Res}(z_n)$  derive from the prefactor of the term  $\propto \delta z^{-1}$  in the expansion

$$\begin{aligned} \frac{e^{\Gamma(z_n + \delta z)}}{\cosh^3(z_n + \delta z)} &= e^{\Gamma z_n} \frac{1 + \Gamma \delta z + \Gamma^2 \delta z^2/2 + \mathcal{O}(\delta z^3)}{-i(-1)^n [\delta z + \delta z^3/6 + \mathcal{O}(\delta z^5)]^3} \\ &= -\frac{e^{\Gamma z_n}}{i\delta z^3} \left[ 1 + \Gamma \delta z + \frac{\Gamma^2 - 1}{2} \delta z^2 + \mathcal{O}(\delta z^3) \right], \end{aligned} \quad (120)$$

and provide us with the following result for the integral in Eq. (119)

$$2\pi i \sum_{n=0}^{\infty} \text{Res}(z_n) = \pi(1 - \Gamma^2) \sum_{n=0}^{\infty} (-1)^n e^{-\Gamma(n + \frac{1}{2})\pi i} \quad (121)$$

$$= \frac{\pi}{2} \frac{1 - \Gamma^2}{\cos(\pi\Gamma/2)} \quad (122)$$

ranging between  $\pi/2$  at  $\Gamma = 0$  and 2 for  $\Gamma = 1$ .

Again, we have to consider the change in the average pinning force  $\langle f_{\text{pin}} \rangle$  when vortices impact the defect at a finite distance  $y$ . The pinning force exerted on a vortex in branch  $i$  passing the defect at an arbitrary transverse distance  $y$  is obtained from Eq. (26),

$$\begin{aligned} f_{\text{pin}}^i(x, y) &= -\frac{\partial}{\partial x} e_{\text{pin}}^i(x, y) \\ &= f_{\text{pin}}^i \left( \sqrt{x^2 + y^2}, 0 \right) \frac{x}{\sqrt{x^2 + y^2}}. \end{aligned}$$

The position of the branch crossing point with equal energies of the pinned and free branches is given by  $x_0(y) = \sqrt{x_0^2 - y^2}$ ; the force exerted at this point is

$$f_{\text{pin}}^i[x_0(y), y] = f_{\text{pin}}^i(x_0, 0) \frac{\sqrt{x_0^2 - y^2}}{x_0} \quad (123)$$

and vanishes at the transverse distance  $y = x_0$ .

The quantity  $\Delta f_{\text{pin}}(x_0)$  is the only term in Eq. (119) that depends on the transverse distance. The frequency factors are independent of  $y$  (they are determined by the asymptotic distance  $|\mathbf{R}|$  of the vortex from the defect, see discussion in Sect. II B). The derivatives  $U_p'$ ,  $U_{\text{dp}}'$  acquire the same  $y$ -dependent factor  $\sqrt{x_0^2 - y^2}/x_0$  as the pinning force in Eq. (123) above, however, this factor is cancelled in the ratio  $\Gamma$ .

Averaging the pinning force  $\Delta f_{\text{pin}}(x_0(y), y)$  over the impact parameter  $|y| < x_0$  results in an additional numerical factor  $\pi/4$  in the expression for the pinning-force density (the fraction of trapped trajectories is  $2x_0/a_0$ ),

$$F_{\text{pin}} = n_p \frac{\langle f_{\text{pin}} \rangle}{a_0} \int_{-x_0}^{x_0} dy \frac{\sqrt{x_0^2 - y^2}}{x_0} = n_p \frac{\pi}{4} \frac{2x_0}{a_0} \langle f_{\text{pin}} \rangle,$$

where  $\langle f_{\text{pin}} \rangle$  is the (thermally) averaged pinning force exerted on vortices passing at  $y = 0$  and calculated through Eq. (115).

Finally, we substitute for the attempt frequencies in Eq. (119) using Eq. (49) and collect the various contributions from above to arrive at the pinning-force density

in the form

$$F_{\text{pin}} = \eta v h(\kappa) (n_p \xi^2 a_0) e^{U_0(\kappa)/T}, \quad (124)$$

with the dimensionless scaling function  $h(\kappa)$

$$h(\kappa) = \frac{\pi^3}{4} \frac{x_0 |\Delta f_{\text{pin}}(x_0)| (\lambda_p/\lambda_f)^{-\Gamma/4}}{\xi^2 |\lambda_{\text{us}}|^{1/2} (\lambda_f \lambda_p)^{1/4}} \frac{1 - \Gamma^2}{\cos(\frac{\Gamma\pi}{2})} \quad (125)$$

accounting for the dependence on the Labusch parameter. At very strong pinning, we use  $\Gamma \approx 1$ ,  $|\Delta f_{\text{pin}}(x_0)| \approx \bar{C}x_0$ , and  $e_p \approx 1/2\bar{C}x_0^2$ , which simplifies  $h(\kappa)$  to

$$h(\kappa) \approx \pi^2 \frac{e_p}{2\xi^2 (|\lambda_{\text{us}}| \lambda_f)^{1/2}} \sim \kappa^{(n+2)/4(n+1)}, \quad (126)$$

while for marginally strong pinning, we find that  $h(\kappa) \sim (\kappa - 1)^{-1/2}$ . Hence, the function  $\tilde{h}(\kappa) = h(\kappa)(\kappa - 1)^{1/2} \kappa^{-(3\alpha+1)/(4\alpha)}$  is roughly constant and ranges between  $\tilde{h}(\infty) \approx 10$  and  $\tilde{h}(0) \approx 22$  (see Fig. 14).

The scaling form of the result (124) can be obtained quite straightforwardly: Using  $p'_{\text{eq}}(x) \approx \delta(x + x_0) - \delta(x - x_0)$  to integrate Eq. (42) provides the estimate  $\langle f_{\text{pin}} \rangle \sim [\ell_{\text{eq}}(x_0)/a_0] \Delta f_{\text{pin}}(x_0)$ . With the transverse trapping distance  $t_{\perp} \sim x_0$ , the pinning force density can be estimated as

$$F_{\text{pin}} \sim n_p \frac{x_0}{a_0} \frac{\ell_{\text{eq}}(x_0)}{a_0} |\Delta f_{\text{pin}}(x_0)|. \quad (127)$$

With the further approximations  $x_0 \sim \xi$ ,  $\Delta f_{\text{pin}}(x_0) \sim e_p/\xi$  and  $\omega_f \sim (e_p/\xi^2)/\eta a_0^3$ , see Eq. (49), we find the result (124) up to the scaling function  $h(\kappa)$ .

The analytical and numerical results for the pinning-force density at low velocities are compared in Fig. 7. Note that the pinning-force density Eq. (124) can be written through the ratio  $v/v_{\text{TAF}}(T)$  using Eq. (79),  $F_{\text{pin}}/F_c = (T/e_p) a(\kappa) h(\kappa) (v/v_{\text{TAF}})$ . Plotting the pinning-force density as a function of  $v/v_{\text{TAF}}(T)$ , see Fig. 7, the additional factor  $T/e_p$  in this expression implies that the upper-most curve corresponds to the highest temperature (this is due to the  $T$ -dependence of  $v_{\text{TAF}}$  itself; if plotting the result as a function of  $v/v_c$ , where  $v_c$  is temperature-independent, the highest pinning force corresponds to the lowest temperature). The numerical results show excellent agreement with the analytic formula for low velocities, while for  $v \sim v_{\text{TAF}}(T)$ , the force dependence crosses over to the logarithmic behaviour as described by Eq. (72).

Finally, we compare our results to those of Brazovskii, Larkin and Nattermann (BLN, Refs.<sup>21,22</sup>). In their study of charge density wave pinning, the pinning-energy landscape is symmetric around the branch crossing point (as is the case for marginally strong vortex pinning, see Appendix A); furthermore, their pinning is effectively one-dimensional, involving no transverse dimensions. Therefore the results of BLN are to be compared to the pinning force  $\langle f_{\text{pin}} \rangle$  calculated for  $\kappa \rightarrow 1$  and  $y = 0$ . BLN neglected the variations of  $p_{\text{eq}}$  about the equal occupation

point  $x_0$ . Using  $p_{\text{eq}}(x) \approx \Theta(x_0 - x)$ , we find their solution for the branch occupation directly by integrating Eq. (113). If  $x < x_0$ , then  $p(x) = 1$  while for  $x > x_0$

$$p_{\text{BN}}(x) = \exp\left[-\int_{x_0}^x \frac{dx'}{\ell_{\text{eq}}(x')}\right] \approx \exp\left[-\frac{x - x_0}{\ell_{\text{eq}}(x_0)}\right], \quad (128)$$

where in the second step, we used the fact that the scale of variations of  $\ell_{\text{eq}}(x)$  is small compared to  $\ell_{\text{eq}}(x_0)$  itself. The solution of BLN thus decays on the short scale  $\ell_{\text{eq}}(x_0)$  while the step in our solution is governed by the variation of  $p_{\text{eq}}(x)$  changing on the larger scale  $T/|\Delta f_{\text{pin}}|$ , see Eq. (C1). Adopting the approximation of BLN, the average pinning force Eq. (115) becomes

$$\langle f_{\text{pin}} \rangle = \nu \frac{|\Delta f_{\text{pin}}(x_0)|}{a_0} \ell_{\text{eq}}(x_0), \quad (129)$$

with the numerical factor  $\nu = 2$  (the result in Ref. [22] is reduced by half since it is calculated per one multivalued interval), however, our result (119) with  $\Gamma(\kappa \rightarrow 1) = 0$  and  $\omega_{\text{dp}} = \omega_p$  results in a different factor  $\nu = \pi/2$ . As the parametric dependence of the area between  $p(x)$  and  $p_{\text{eq}}(x)$  turns out to be the same in BLN and in our case, the results differ only by a numerical factor. Our result (119) for  $\langle f_{\text{pin}} \rangle$  thus provides a more accurate and universal (as it deals with non-symmetric pinning landscapes) result than BLN.

#### 4. Current-velocity characteristic

Inserting the result (124) for the pinning-force density  $F_{\text{pin}}$  back to the equation of motion (1) provides the current-voltage characteristic at small velocities  $v \ll v_{\text{TAFF}} = v_{\text{th}} e^{-U_0/T}$ ,

$$\frac{v}{v_c} \left[ 1 + h(\kappa) n_p a_0 \xi^2 e^{U_0/T} \right] = \frac{j}{j_c}. \quad (130)$$

The exponential term dominates for low temperatures,  $T \ll U_0/|\ln[h(\kappa) n_p a_0 \xi^2]|$  and the slope of the characteristic is exponentially suppressed compared to the slope  $v_c/j_c$  describing free flux-flow,

$$v = \frac{v_c}{j_c} \frac{\exp(-U_0/T)}{h(\kappa) n_p a_0 \xi^2} j. \quad (131)$$

The activation barrier  $U_0$  does not depend on  $j$  but remains constant, see Eq. (C4), different from the weak collective pinning scenario where the creep barriers  $U(j) \propto j^{-\mu}$  diverge as  $j \rightarrow 0$ . As a result, the glassy response of a true superconductor in the weak collective pinning framework is replaced by a resistive normal metallic behavior in the strong pinning setting. The exponential reduction of the normal resistance is known under the name TAFF, thermally assisted flux flow<sup>34</sup>. The crossover to high velocities with a non-linear characteristic at  $v_{\text{TAFF}} = v_{\text{th}} e^{-U_0/T}$  is realized at the driving current  $j_{\text{TAFF}} = (v_{\text{th}}/v_c) h(\kappa) (n_p a_0 \xi^2) j_c = a(\kappa) h(\kappa) (T/e_p) j_c$ .

## IV. SUMMARY AND CONCLUSION

Including thermal fluctuations into the strong pinning paradigm, we have advanced this quantitative theory of pinning by a further important step. As a result, we have arrived at a rather comprehensive picture of strong pinning that provides us with the critical current density<sup>16</sup>, the current-voltage characteristic<sup>11,12</sup>, and its smoothing due to thermal fluctuations. Furthermore, the parametric conditions for the validity of strong pinning theory have been identified<sup>16</sup>. An important result of the present study is the obtained insight on the form of the current-voltage characteristic which is of the excess-current form—thermal fluctuations leave this simple form essentially unchanged. From this finding, we conclude that pinning and creep are preserved when driving the system above the critical current density  $j_c$ . This is in contrast to the usual perception of a steep rise in dissipation appearing above  $j_c$ , an expectation that may be understood in terms of avalanche formation. The strong pinning paradigm, though, is rather in agreement with Coulomb's law of dry friction, telling that the friction force remains unchanged when motion sets in.

The present work provides us with a precise prediction for the current-voltage characteristic at finite temperatures. We have found that the role of  $j_c$  is taken over by the depinning current density  $j_{\text{dp}}(T)$  separating flat and steep regions of the characteristic, with  $j_{\text{dp}}(T)$  reduced with respect to  $j_c$  by a term  $\propto (T/e_p)^{2/3}$ , see Eq. (91). Below  $j_{\text{dp}}(T)$ , vortex motion is determined by creep over barriers  $U(j) \approx U_c(1 - j/j_c)^{3/2}$ , see Eq. (93). The exponent 3/2 is universal for smooth pinning potentials and derives from the exponent describing the vanishing of depinning and pinning barriers at the boundaries of the bistable region  $[x_-, x_+]$ , see Eq. (55). The motion above  $j_{\text{dp}}(T)$  is flux-flow like until joining the  $T = 0$  characteristic at  $v_{\text{th}} \sim (T/e_p) \kappa v_p$ ,  $v_p \sim f_p/a_0^3 \eta$  the velocity scale for vortex motion within a pinning well. Formulating this flow-type motion through barriers, the latter exhibit a weak logarithmic dependence on  $j$ , see Eq. (97), and hence a linear rise in dissipation.

Creep barriers are conveniently measured through relaxation experiments; our result with the 3/2 exponent in the activation barriers provides us with the normalized creep rate  $S(T, t)$  in Eq. (104) with an initial non-linear and convex increase with temperature  $T$  that transforms into a concave shape at higher temperatures; as a result, the relaxation rate  $S(T)$  exhibits an inflection point. Finally, the temperature scale where pinning stops suppressing the flow-type vortex motion is given by the thermal depinning temperature  $T_{\text{dp}}$  that is of order  $e_p$ , see Eq. (87). Focussing the discussion on low drives  $v < v_{\text{TAFF}} = v_{\text{th}} e^{-U_0/T}$  with  $U_0$  the maximal barrier appearing at the branch cutting point, we have found a quantitative result for the thermally assisted flux-flow characteristic  $v/v_c \propto e^{-U_0/T} (j/j_c)$ , see Eq. (131).

Several findings in the present paper are amenable to experimental verification, foremost, the thermal modi-

fications of the excess-current characteristics predicted by strong pinning theory. Although systematic data is scarce, we have found that transport experiments on NbSe<sub>2</sub><sup>41,42</sup> and on MoGe<sup>43,44</sup> can be successfully analyzed in terms of our strong pinning theory; we will devote a separate publication to this topic<sup>45</sup>. Regarding creep rates, indications for an inflection point have been reported in experiments on pnictide and cuprate superconductors<sup>38</sup>. Finally, thermally assisted flux-flow has been experimentally observed and quantitatively analyzed in high temperature superconductors<sup>46–48</sup>.

Within the strong pinning paradigm, pinning due to individual defects is finite. As  $\kappa$  drops below unity, individual pins cannot hold a vortex any longer (since the energy landscape is single valued and hence the jumps  $\Delta e_{\text{pin}} = 0$  vanish). As a result, collective pinning effects due to multiple defects have to be included in the pinning analysis around  $\kappa \simeq 1$ . This is also the case when the current drive vanishes or approaches its critical value—in both cases corrections from neighboring defects become important and hence our results will get modified in these regimes. Other topics of interest are the decay of lattice order<sup>49</sup> and the physics of one-dimensional strong pinning, a regime enclosed between 3D strong pinning and 1D weak collective pinning within the pinning diagram of Ref. [16], and future work will address several of these issues.

## ACKNOWLEDGMENTS

We thank Eva Andrei, Alexei Koshelev, Zhi-Li Xiao, and Eli Zeldov for illuminating discussions and acknowledge financial support of the Swiss National Science Foundation, Division II and the PostDoc Mobility fellowship (R.W.).

## Appendix A: Marginally strong pinning

At marginally strong pinning, the slope  $\bar{C}$  is close to (but smaller than) the maximum slope of the bare pinning force  $f_p(r)$  and the multivalued solutions for the tip position  $r(x)$  reside in the vicinity of the inflection point  $r_m$ ,  $f_p''(r_m) = 0$ , see Fig. 12. The characteristics of the pinning energy landscape then can be obtained from an expansion of the pinning force around  $r_m$ ,

$$f_p(r_m + \delta r) = f_p(r_m) + \kappa \bar{C} \delta r - \frac{1}{3} \gamma \delta r^3 + \dots \quad (\text{A1})$$

with  $\kappa \bar{C} = f_p'(r_m)$ , see Eq. (14), and the third derivative  $\gamma = -f_p'''(r_m)/2 > 0$ ,  $\gamma \sim f_p/\xi^3$ . As long as the higher order terms in (A1) can be neglected, the bare pinning force is antisymmetric about the inflection point,

$$f_p(r_m + \delta r) - f_p(r_m) = -[f_p(r_m - \delta r) - f_p(r_m)]. \quad (\text{A2})$$

The line with slope  $\bar{C}$  passing through the inflection point defines the asymptotic vortex position  $x_m$  related to  $r_m$ ,

$x_m = r_m - f_p(r_m)/\bar{C}$ , see Eq. (15) and Fig. 12. The symmetry property (A2) implies that  $x_m = (x_+ + x_-)/2$ .

Making use of the relation (A2), we determine the derivatives of the pinning energy for the branches  $i = p, f$  of the multi-valued energy landscape, see Eq. (13),

$$\begin{aligned} \frac{d}{dx} e_{\text{pin}}^i(x) &= \frac{d}{dx} e_{\text{pin}}[x, r_i(x)] = -f_p[r_i(x)] r_i'(x) \quad (\text{A3}) \\ &+ \bar{C}[r_i(x) - x][r_i'(x) - 1] = -f_p[r_i(x)] = -f_{\text{pin}}^i(x). \end{aligned}$$

Subtracting the slope  $(x - x_m)f_p(r_m)$  from  $e_{\text{pin}}^i(x)$ , we obtain the symmetrized energy landscape

$$e_{s,\text{pin}}^i(x) \equiv e_{\text{pin}}^i(x) + (x - x_m)f_p(r_m), \quad (\text{A4})$$

symmetric around the branch crossing point at  $x_m$ , see Fig. 12. In particular, the difference in the tilted energies  $e_{s,\text{pin}}^i(x)$  between the points  $B'$  and  $B$  (as defined in the force diagram of Fig. 12) can be expressed as an integral from  $r_+$  to  $r_-$ ; this quantity vanishes due to the symmetry (A2),

$$e_{\text{pin}}^p(x_m) - e_{\text{pin}}^f(x_m) = \int_B^{B'} dx \{-f_p[r(x)] + f_p(r_m)\} = 0,$$

implying that  $x_m$  indeed corresponds to the branch crossing point,  $x_m = x_0$ . Differentiating Eq. (15) and evaluating the second derivative  $d^2 e_{\text{pin}}^i(x)/dx^2$  gives

$$\frac{d^2 e_{\text{pin}}^i(x)}{dx^2} = \frac{\bar{C}}{1 - \bar{C}/f_p'[r_i(x)]}. \quad (\text{A5})$$

We conclude that the energy landscape is concave for the pinned and free branches (for which the curvature  $\lambda_{p,f} = \bar{C} - f_p'[r_i(x)] > 0$ ) and convex for the unstable branch for which  $\lambda_{\text{us}} < 0$ .

All quantities characteristic for strong pinning, such as the bistable region  $[x_-, x_+]$ , the jumps  $\Delta e_{\text{pin}}(x_{\pm})$ , the energy barriers  $U_{p,\text{dp}}(x)$ , etc., must vanish at the crossover point  $\kappa = 1$ ; they scale with a power of the small parameter  $\kappa - 1$ . In particular, as a straightforward calculation shows, we find the extremal tip locations  $r_{\pm} = r_m \mp \delta r_{\text{max}}$  from the condition  $f_p'(r_{\pm}) = \bar{C}$ ,

$$\delta r_{\text{max}} = \sqrt{\frac{\bar{C}}{\gamma}} (\kappa - 1)^{1/2} \sim (\kappa - 1)^{1/2} \xi \quad (\text{A6})$$

from which the end-points  $x_{\pm} = x_m \pm \delta x_{\text{max}}$  of the multi-valued interval appear at

$$\delta x_{\text{max}} = \frac{2}{3} \sqrt{\frac{\bar{C}}{\gamma}} (\kappa - 1)^{3/2} \sim (\kappa - 1)^{3/2} \xi, \quad (\text{A7})$$

see (46), with the dimensional estimate  $\gamma \sim f_p/\xi^3$  and  $\kappa \sim 1$  used in the last relation.

The results for the curvatures, barriers, and frequency factors near the multi-valued interval end points  $x_{\pm}$  are



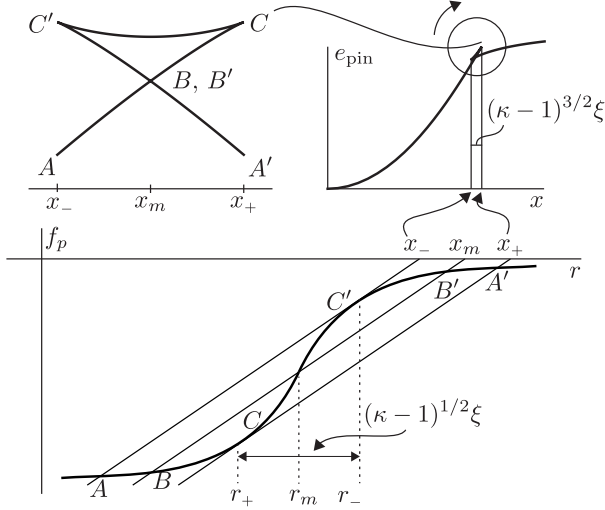


FIG. 12. In the marginally strong pinning regime, the energy landscape is fully characterized by an expansion of the bare pinning force (bottom) around the inflection point  $r_m$  up to the order  $(r_m - r)^3$ . The pinning force is locally symmetric around the inflection point  $r_m$ , which gives rise to the symmetric pinning energy landscape  $e_{s, \text{pin}}^i(x)$  (top left) and implies that  $x_m = r_m - f_p(r_m)/\bar{C}$  corresponds to the branch crossing point  $x_0$ ,  $x_m = x_0$ .

obtained using  $f_p''(r_+) = -f_p''(r_-) = 2\gamma\delta r_{\text{max}}$ ,

$$\lambda_{f, \text{us}}(x_- + \delta x) = \pm \sqrt{\frac{8}{3}}(\kappa - 1)\bar{C} \left( \frac{\delta x}{\delta x_{\text{max}}} \right)^{1/2}, \quad (\text{A8})$$

$$U_p(x_- + \delta x) = \frac{4\bar{C}^2}{3\gamma}(\kappa - 1)^2 \left( \frac{2\delta x}{3\delta x_{\text{max}}} \right)^{3/2}, \quad (\text{A9})$$

$$\omega_f(x_- + \delta x) = \frac{\bar{C}}{2\pi\eta a_0^3} \sqrt{\frac{8}{3}}(\kappa - 1) \left( \frac{\delta x}{\delta x_{\text{max}}} \right)^{1/2}, \quad (\text{A10})$$

and corresponding results hold for  $\lambda_{p, \text{us}}$ ,  $U_{\text{dp}}$ , and  $\omega_p$  evaluated at  $x_+ - \delta x$ .

In order to find the force jumps  $\Delta f_{\text{pin}}(x_+) = -\Delta f_{\text{pin}}(x_-)$ , we first determine the tip location  $r_f$  of the free solution at the interval end point,  $r_f(x_+) = r_m + 2\delta r_{\text{max}}$ ; then

$$\begin{aligned} \Delta f_{\text{pin}}(x_+) &= f_p(r_m - \delta r_{\text{max}}) - f_p(r_m + 2\delta r_{\text{max}}) \\ &= -3\bar{C} \sqrt{\frac{\bar{C}}{\gamma}}(\kappa - 1)^{1/2} \sim -f_p(\kappa - 1)^{1/2}. \end{aligned} \quad (\text{A11})$$

A more lengthy calculation yields the energy jumps<sup>8,16</sup>

$$\begin{aligned} \Delta e_{\text{pin}}(x_+) &= e_p(r_+) + \frac{1}{2}\bar{C}(x_+ - r_+)^2 - e_p[r_f(x_+)] \\ &- \frac{1}{2}\bar{C}(x_+ - r_f(x_+))^2 = \frac{9\bar{C}^2}{4\gamma}(\kappa - 1)^2 \end{aligned} \quad (\text{A12})$$

and  $\Delta e_{\text{pin}}(x_-) = -\Delta e_{\text{pin}}(x_+)$ .

Next, we determine various quantities at the branch crossing point  $x_0 = x_m$ . The three solutions for the tip locations  $r_i(x)$  at the branch crossing point are  $r_{\text{us}}(x_m) = r_m$  and  $r_{p, f}(x_m) = r_m \mp \sqrt{3}\delta r_{\text{max}}$ . Using Eq. (50), we find the curvatures and attempt frequencies

$$\lambda_{\text{us}}(x_0) = -\bar{C}(\kappa - 1), \quad \lambda_{p, f}(x_0) = \frac{\bar{C}}{2}(\kappa - 1), \quad (\text{A13})$$

$$\omega_f(x_0) = \omega_p(x_0) = \frac{\bar{C}(\kappa - 1)}{2\pi\sqrt{2}\eta a_0^3}. \quad (\text{A14})$$

The force difference between pinned and free branches is

$$\Delta f_{\text{pin}}(x_0) = -2\bar{C} \sqrt{\frac{3\bar{C}}{\gamma}}(\kappa - 1)^{1/2}, \quad (\text{A15})$$

the energy difference  $\Delta e_{\text{pin}}(x_0)$  vanishes. The maximum energy barrier  $U_0 = U_{\text{dp}}(x_0) = U_p(x_0)$  is

$$\begin{aligned} U_0 &= e_{\text{pin}}(x_0, r_m) - e_{\text{pin}}(x_0, r_m + \delta r_0) \\ &= \frac{3\bar{C}^2}{4\gamma}(\kappa - 1)^2. \end{aligned} \quad (\text{A16})$$

We further calculate the various scaling functions discussed in the text. The coefficients  $\kappa_{\pm}$  appearing in the curvatures and barrier expansions (51)–(56) read

$$\kappa_{\pm} = \xi \sqrt{\frac{\gamma}{\bar{C}}}(\kappa - 1)^{1/2} \sim (\kappa - 1)^{1/2}. \quad (\text{A17})$$

The scaling function  $g(\kappa)$  appearing in the pinning-force density  $F_{\text{pin}}$ , see Eq. (76), takes the form

$$g(\kappa) = \left[ \frac{4\gamma^2 e_p^2}{3(\kappa - 1)^4 \bar{C}^4} \right]^{1/3} \sim \frac{1}{(\kappa - 1)^{4/3}}, \quad (\text{A18})$$

and the function  $a(\kappa)$  entering the characteristic at high velocities, see Eq. (81), is given by

$$a(\kappa) = \frac{1}{9\pi} \frac{e_p \xi^2}{x_m \bar{C}} \left( \frac{\gamma/\bar{C}}{\kappa - 1} \right)^{3/2} \sim \frac{1}{(\kappa - 1)^{3/2}}. \quad (\text{A19})$$

The pinning-force density  $F_{\text{pin}}$  at low velocities involves the scaling function  $h(\kappa)$  of Eq. (125),

$$h(\kappa) \approx \frac{\pi^2 \sqrt{6}}{4} \frac{x_0}{\xi^2} \left( \frac{\bar{C}/\gamma}{\kappa - 1} \right)^{1/2} \sim \frac{1}{(\kappa - 1)^{1/2}}. \quad (\text{A20})$$

## Appendix B: Very strong pinning

When pinning is very strong, i.e., the slope  $\bar{C}$  is small compared to the maximum slope of  $f_p(r)$ , see Fig. 13, the relevant expansions of the pinning force are around the origin when investigating the pinned branch and in the tail when dealing with the free branch. Here, we discuss

the pinning energy for bare pinning potentials  $e_p(r)$  decaying on a scale  $\xi$  from its minimal value  $-e_p = e_p(0)$ . The induced pinning force  $f_p(r) = -e_p'(r)$  quickly reaches its maximal value  $f_p \sim e_p/\xi$  on the distance of the vortex core size  $r \sim \xi$ . We assume an algebraically decaying tail of the bare pinning potential,  $e_p(r) \sim -e_p(r/\xi)^{-n}$ ,  $r \gg \xi$ , for instance,  $n = 2$  for the commonly-used Lorentzian pinning potential

$$e_p(r) = -\frac{e_p}{1 + r^2/2\xi^2}. \quad (\text{B1})$$

Whenever convenient, we will make use of the parametric dependence  $\kappa \sim f_p/\bar{C}\xi \sim e_p/\bar{C}\xi^2$ . The pinning energy profile  $e_{\text{pin}}(x; r)$  in Fig. 2 involves the superposition of a shallow (elastic) parabola  $\bar{C}(r-x)^2/2$  centered at  $r = x$  and a narrow bare pinning potential  $e_p(r)$  centered at the origin. For  $x = 0$  the vortex is placed directly at the pinning center and  $e_{\text{pin}}(r)$  has only one minimum  $r_p = 0$  corresponding to the pinned branch. A second minimum with a tip position at  $r_f(x)$  appears at the point  $x_-$ . Since the point  $r_- = r_f(x_-)$  lies on the tail of the bare pinning force  $f_p(r)$ , evaluating the condition  $f_p'(r_-) = \bar{C}$  gives  $r_- \sim \xi\kappa^{1/(1+n)}$ . The corresponding asymptotic position of the vortex is  $x_- = r_- - f_p(r_-)/\bar{C} \sim \xi\kappa^{1/(1+n)}$ .

The new (free) minimum becomes deeper as the asymptotic position  $x$  is further increased away from the defect. Both minima are of equal energy at the branch-crossing point when  $\bar{C}x_0^2/2 \approx e_p$  and hence  $x_0 \approx \sqrt{2e_p/\bar{C}} \sim \kappa^{1/2}\xi$ . Finally, the original (pinned) minimum disappears for very large  $x$  when the slope of the parabola balances the maximum pinning force  $\bar{C}x_+ \approx f_p$  and we obtain  $x_+ \sim \kappa\xi$ .

To evaluate the scaling form of curvatures, barriers, and frequencies near the end points  $x_+$  and  $x_-$  of the multivalued interval, we use Eqs. (51)–(56) with  $f_p''(r_-) \sim (f_p/\xi^2)\kappa^{-\nu}$ ,  $\nu = (n+2)/(n+1)$  and  $f_p''(r_+) \sim (f_p/\xi^2)$ . As a result, we find a different behavior of the barriers and curvatures near the two end points  $x_{\pm}$ ,

$$\begin{aligned} \lambda_{f,\text{us}}(x_- + \delta x_-) &\sim \pm \frac{e_p}{\kappa^{\nu/2}\xi^2} \left( \frac{\delta x_-}{\kappa\xi} \right)^{1/2}, \\ \lambda_{p,\text{us}}(x_+ - \delta x_+) &\sim \pm \frac{e_p}{\xi^2} \left( \frac{\delta x_+}{\kappa\xi} \right)^{1/2}, \end{aligned} \quad (\text{B2})$$

and

$$\begin{aligned} U_p(x_- + \delta x_-) &\sim e_p \kappa^{\nu/2} \left( \frac{\delta x_-}{\kappa\xi} \right)^{3/2}, \\ U_{\text{dp}}(x_+ - \delta x_+) &\sim e_p \left( \frac{\delta x_+}{\kappa\xi} \right)^{3/2}. \end{aligned} \quad (\text{B3})$$

Note the additional large factor  $\kappa^{\nu/2}$  that appears in connection with quantities evaluated near  $x_-$ .

For positions  $x$  far away from the boundaries  $x_{\pm}$ , the curvatures are dominated either by the shallow parabolic well with  $\lambda_f(x \gg x_-) \approx \bar{C} \sim e_p/\kappa\xi^2$  on the free branch

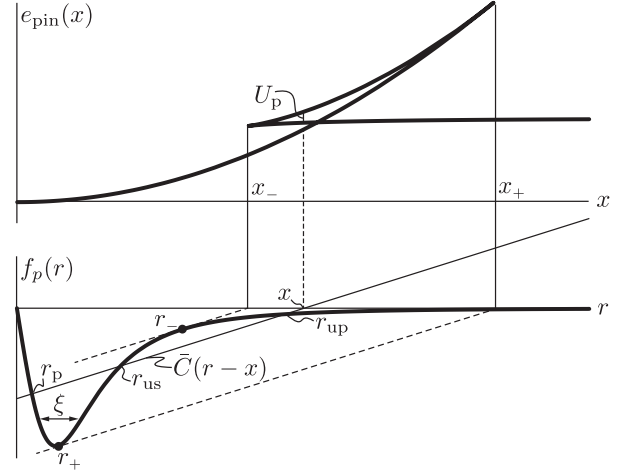


FIG. 13. For very strong pinning with  $\kappa \gg 1$ , the slopes  $f_p'(r)$  are steep compared to the slope  $\bar{C}$  of the elastic restoring force. This results in an extended multistable region between  $x_- \sim \xi\kappa^{1/(1+n)}$  and  $x_+ \sim \kappa\xi$ , wherein the tip positions of the free and pinned states assume values  $r_f \approx x$  and  $r_p \sim x/\kappa$ , while the unstable solution lies between  $r_+ \sim \xi$  and  $r_- \sim \kappa^{1/(1+n)}\xi$ . The extent of the multivalued region is  $x_+ - x_- \sim \kappa\xi$ .

or by the narrow pinning potential well on the pinned branch,  $\lambda_p(x \ll x_+) \approx e_p''[r_p(x)] \sim e_p/\xi^2$ . For the unstable solution, we have  $r_{\text{us}}(x) < r_- \ll x$  and hence  $r_{\text{us}}$  resides in the tail of  $f_p(x)$  for  $x \ll x_+$ . Then, the equilibrium Eq. (15) reads  $\bar{C}x \sim f_p(r_{\text{us}}/\xi)^{-n}$  and  $r_{\text{us}} \sim \xi(x/\kappa\xi)^{-1/n}$ . Evaluating the curvature in this situation, we find that  $\lambda_{\text{us}}(x) \sim -(e_p/\xi^2)(x/\kappa\xi)^{(n+1)/n}$ . The scaling forms for the frequency factors follow from Eq. (49) and are summarized in Table I.

In order to find the barrier near the branch crossing point  $x_0$ , we make use of Eq. (A3) and integrate away from  $x_-$ ,

$$U_p(x) = \int_{x_-}^x dx' \{f_p[r_f(x')] - f_p[r_{\text{us}}(x')]\}. \quad (\text{B4})$$

Using the equilibrium condition (15) for the tip position and  $r_f(x) \approx x$ , this simplifies to

$$\begin{aligned} U_p(x) &= \bar{C} \int_{x_-}^x dx' [r_f(x') - r_{\text{us}}(x')] \\ &\approx \frac{1}{2}\bar{C}(x^2 - x_-^2) - \bar{C} \int_{x_-}^x dx' r_{\text{us}}(x'). \end{aligned} \quad (\text{B5})$$

We make use of the scaling form of  $r_{\text{us}}(x)$  derived above and note that the integral is dominated by its upper boundary, resulting in

$$\frac{1}{2}\bar{C}(x^2 - x_-^2) - U_p(x) = \mu e_p \left( \frac{x}{\kappa\xi} \right)^{(n-1)/n}, \quad (\text{B6})$$

where  $\mu$  is a  $\kappa$ -independent numerical. The barrier  $U_0 = U_p(x_0)$  at the branch crossing point  $x_0 \sim \kappa^{1/2}\xi$  then is

given by

$$U_0 \sim \bar{C} \kappa \xi^2 \sim e_p, \quad (\text{B7})$$

with corrections of order  $\sim -e_p/\kappa^{(n-1)/2n}$ .

### Appendix C: Equilibrium properties

We discuss the properties of the equilibrium occupation  $p_{\text{eq}}$  and the relaxation length  $\ell_{\text{eq}}$  and expand both quantities around the branch crossing point  $x_0$ . Expanding  $\Delta e_{\text{pin}}(x_0 + \delta x) \approx -\Delta f_{\text{pin}}(x_0)\delta x$  in the exponential and neglecting the change in the frequency factors provides a good approximation of  $p_{\text{eq}}(x)$  in the entire multi-valued interval; when the change in the frequency factors becomes significant ( $\omega_{\text{p,up}}$  vary on the scale  $\kappa\xi$  of the multi-valued interval), the occupation is already completely dominated by the exponential (which changes on a short scale  $T/|\Delta f_{\text{pin}}(x_0)|$ ). We thus can rewrite Eq. (108) as

$$\begin{aligned} p_{\text{eq}}(x_0 + \delta x) &\approx \frac{1}{2} + \frac{1 - (\omega_{\text{p}}/\omega_{\text{f}})e^{-\Delta f_{\text{pin}}\delta x/T}}{2[1 + (\omega_{\text{p}}/\omega_{\text{f}})e^{-\Delta f_{\text{pin}}\delta x/T}]} \\ &= \frac{1}{2} - \frac{1}{2} \tanh\left[\frac{1}{2} \ln \frac{\omega_{\text{p}}}{\omega_{\text{f}}} - \frac{\Delta f_{\text{pin}}}{2T} \delta x\right]. \end{aligned} \quad (\text{C1})$$

The force difference between the branches scales as  $\Delta f_{\text{pin}} \sim -f_{\text{p}}(\kappa - 1)^{1/2}$ ,  $-f_{\text{p}}\kappa^{-1}$  in the limit of marginally and very strong pinning. The ratio of frequency factors is  $\omega_{\text{p}}/\omega_{\text{f}} = \lambda_{\text{p}}/\lambda_{\text{f}} \sim \sqrt{\kappa}$  for very strong pinning and reaches unity if pinning is marginally strong. Determining the point of equal branch occupation  $p_{\text{eq}}(x_{\text{eo}}) = 1/2$ , we then find it shifted to the left from the branch crossing point,

$$x_{\text{eo}} \approx x_0 + \frac{T}{\Delta f_{\text{pin}}} \ln \frac{\omega_{\text{p}}}{\omega_{\text{f}}} \Big|_{x_0} \approx x_0 + \frac{T \ln \kappa}{2\Delta f_{\text{pin}}(x_0)}. \quad (\text{C2})$$

This shift is comparable to the scale  $T/|\Delta f_{\text{pin}}|$  of variations in  $p_{\text{eq}}(x)$  but is small (at low temperatures) compared to the extension of the pinning landscape.

Next, we wish to understand the local behavior of  $\ell_{\text{eq}}(x)$  around  $x_0$ . We expand the depinning and pinning barriers in Eq. (41) around  $x_0$ ,  $U_{\text{p,dp}} = U_0 + U'_{\text{p,dp}}(x_0)\delta x$  and neglect variations of the attempt frequencies  $\omega_{\text{p,f}}(x)$ ,

$$\ell_{\text{eq}}(x_0 + \delta x) \approx \frac{v e^{U_0/T}}{\omega_{\text{p}} e^{-U'_{\text{dp}}\delta x/T} + \omega_{\text{f}} e^{-U'_{\text{p}}\delta x/T}}. \quad (\text{C3})$$

The maximal barrier  $U_0$  at  $x_0$  is given by

$$U_0 = e_{\text{pin}}(x_0, r_{\text{us}}) - e_{\text{pin}}(x_0, r_{\text{p}}) \quad (\text{C4})$$

and vanishes as  $e_{\text{p}}(\kappa - 1)^2$  for marginally strong pinning, while assuming a value of order  $e_{\text{p}}$  with corrections of order  $e_{\text{p}}/\kappa^{n/(2n+2)}$  at very strong pinning, see Appendix B. For marginally strong pinning, the slopes of the barriers have equal magnitude,  $U'_{\text{p}}(x_0) = -U'_{\text{dp}}(x_0)$  while for

very strong pinning, we have  $r_{\text{p}} \sim \xi/\kappa$ ,  $r_{\text{f}} \sim x$ , and  $r_{\text{us}} \sim \xi(x/\kappa\xi)^{-1/\alpha}$  with  $x = x_0 \sim \kappa^{1/2}\xi$ . This provides us with the ratio

$$\frac{|U'_{\text{dp}}|}{U'_{\text{p}}} = \frac{f_{\text{pin}}^{\text{us}} - f_{\text{pin}}^{\text{p}}}{f_{\text{p}}^{\text{f}} - f_{\text{p}}^{\text{us}}} = \frac{\bar{C}(r_{\text{us}} - r_{\text{p}})}{\bar{C}(r_{\text{f}} - r_{\text{us}})} \sim \frac{\kappa^{1/2(n+1)}}{\kappa^{1/2}} \quad (\text{C5})$$

with  $n$  the exponent describing the tails of the pinning energy relevant for very strong pinning.

Maximizing the equilibrium relaxation length (C3) with respect to  $\delta x$  then provides us with the location  $x_{\text{lr}}$  of the longest relaxation length,

$$x_{\text{lr}} - x_0 \approx \frac{T}{\Delta f_{\text{pin}}} \ln \frac{\omega_{\text{p}}}{\omega_{\text{f}}} \frac{|U'_{\text{dp}}|}{U'_{\text{p}}} \Big|_{x_0} \sim \frac{T \ln \kappa}{2(n+1)\Delta f_{\text{pin}}}, \quad (\text{C6})$$

with  $n$  the exponent describing the tails of the pinning energy relevant for very strong pinning. Note that the maximum relaxation length  $\ell_{\text{eq}}(x_{\text{lr}})$  does not differ significantly from its value at the point  $x_0$ . Substituting Eq. (C6) to Eq. (C3) provides the estimate  $\ell_{\text{eq}}(x_{\text{lr}}) \sim \ell_{\text{eq}}(x_0)\kappa^\alpha$  with a small exponent  $\alpha = |U'_{\text{dp}}|/[2(n+1)|\Delta f_{\text{pin}}|] \sim \kappa^{1/2(n+1)-1/2}/2(n+1)$  at very strong pinning (we use  $\omega_{\text{p}}/\omega_{\text{f}} \sim \sqrt{\kappa}$ ). As a result, we find that the various positions  $x_0$ ,  $x_{\text{eo}}$ , and  $x_{\text{lr}}$  are arranged in the sequence  $x_{\text{eo}} < x_{\text{lr}} < x_0$ , see Fig. 11 and note that  $\Delta f_{\text{pin}} < 0$ ; for marginally strong pinning  $\kappa \rightarrow 1$ , the energy landscape becomes symmetric and  $x_{\text{eo}} = x_{\text{lr}} = x_0$ .

Finally, we analyze the decay of  $\ell_{\text{eq}}$  away from its maximum. We note that for  $x > x_0$ ,  $U_{\text{dp}}(x) < U_{\text{p}}(x)$  and therefore at small temperatures  $\ell_{\text{dp}}(x) \ll \ell_{\text{p}}(x)$ , resulting in  $\ell_{\text{eq}}(x) \approx \ell_{\text{dp}}(x) \propto e^{U_{\text{dp}}(x)/T}$  and thus  $\ell_{\text{eq}}(x)$  decays on the scale  $T/|U'_{\text{dp}}|$  to the right of its maximum. Similarly if  $x < x_0$ ,  $\ell_{\text{eq}}(x) \approx \ell_{\text{p}}(x) \propto e^{U_{\text{p}}(x)/T}$  and thus  $\ell_{\text{eq}}$  grows on approaching  $x_0$  from the left on the different scale  $T/U'_{\text{p}}$ , see the inset of Fig. 11. For very strong pinning, the ratio of growth and decay is  $|U'_{\text{dp}}|/U'_{\text{p}} < 1$ , see Eq. (C5), while for marginally strong pinning the growth and decay scales are identical.

### Appendix D: Current-velocity characteristic

#### 1. Iteration scheme

We solve the equation (78),

$$\frac{v}{v_{\text{th}}} = \frac{1}{\mathcal{A}} \frac{\delta j}{j_c} + \frac{1}{\nu} \left[ \ln \frac{v_{\text{th}}}{v} \right]^{2/3} \quad (\text{D1})$$

for the current-velocity characteristic at the point  $\delta j = 0$  corresponding to the critical drive. The iteration procedure for the solution  $x = v(j_c)/v_{\text{th}}$  is given by

$$x_0 = 1/\nu, \quad x_{n+1} = \frac{[\log(1/x_n)]^{2/3}}{\nu}. \quad (\text{D2})$$

The condition  $\nu > 1$  is not sufficient to ensure positivity of all logarithms. For instance, if we consider  $\nu = 1 + \varepsilon$ ,

with  $\varepsilon$  a small correction, we find that the logarithm in  $x_3$  becomes negative,

$$x_0 \approx 1 - \varepsilon, \quad (\text{D3})$$

$$x_1 \approx \varepsilon^{2/3}, \quad (\text{D4})$$

$$x_2 \approx \left(\frac{2}{3} \log \frac{1}{\varepsilon}\right)^{2/3}, \quad (\text{D5})$$

$$x_3 \approx \left[\frac{2}{3} \log \frac{1}{(\frac{2}{3} \log 1/\varepsilon)^{2/3}}\right]^{2/3}. \quad (\text{D6})$$

In fact, the iterative procedure can converge to the true solution  $x^*$  of  $x = (1/\nu)[\ln(1/x)]^{2/3}$  only if

$$\left| \frac{\partial}{\partial x} \frac{[\ln(1/x)]^{2/3}}{\nu} \right|_{x=x^*} < 1, \quad (\text{D7})$$

$$\frac{2}{3\nu x^* [\ln(1/x^*)]^{1/3}} = \frac{2}{3 \ln(1/x^*)} < 1, \quad (\text{D8})$$

i.e., the solution must satisfy  $x^* < e^{-2/3} \equiv x_{\text{lim}}$ . Substituting back to the equation fixing  $x^*$ , we find the limiting value of  $\nu$ ,

$$\nu_{\text{lim}} = \frac{1}{x_{\text{lim}}} \left( \ln \frac{1}{x_{\text{lim}}} \right)^{2/3} = \left( \frac{2e}{3} \right)^{2/3} \approx 1.49. \quad (\text{D9})$$

Results for Eq. (D1) at large and small values of  $\nu$  are given in the main text, see Eqs. (84) and (85).

## 2. Depinning current

The definition of the depinning current density  $j_{\text{dp}}(T)$  as the point of steepest change in the differential resistivity leads to the condition  $\partial^3 v / \partial j^3 = 0$ . Assuming that we know the expression  $j(v)$ , we need to use the chain rule repeatedly to arrive at

$$\begin{aligned} \frac{\partial v}{\partial j} &= \left( \frac{\partial j}{\partial v} \right)^{-1}, \\ \frac{\partial^2 v}{\partial j^2} &= \frac{\partial}{\partial v} \left[ \left( \frac{\partial j}{\partial v} \right)^{-1} \right] \left( \frac{\partial j}{\partial v} \right)^{-1} = - \left( \frac{\partial j}{\partial v} \right)^{-3} \frac{\partial^2 j}{\partial v^2}, \\ \frac{\partial^3 v}{\partial j^3} &= - \frac{\partial}{\partial v} \left[ \left( \frac{\partial j}{\partial v} \right)^{-3} \frac{\partial^2 j}{\partial v^2} \right] \left( \frac{\partial j}{\partial v} \right)^{-1} \\ &= 3 \left( \frac{\partial j}{\partial v} \right)^{-5} \left( \frac{\partial^2 j}{\partial v^2} \right)^2 - \left( \frac{\partial j}{\partial v} \right)^{-4} \frac{\partial^3 j}{\partial v^3}. \end{aligned} \quad (\text{D10})$$

The condition  $\partial^3 v / \partial j^3 = 0$  is thus equivalent to

$$\frac{\partial^3 j}{\partial v^3} \frac{\partial j}{\partial v} = 3 \left( \frac{\partial^2 j}{\partial v^2} \right)^2. \quad (\text{D11})$$

Substituting Eq. (78) leads to the condition ( $x = v_{\text{dp}}/v_{\text{th}}$ )

$$\begin{aligned} 54\nu x [\ln(1/x)]^{7/3} - 27\nu x [\ln(1/x)]^{4/3} + 12\nu x [\ln(1/x)]^{1/3} \\ - 18[\ln(1/x)]^2 + 18 \ln(1/x) + 2 = 0. \end{aligned} \quad (\text{D12})$$

We expect  $x \lesssim 1/\nu$ , with  $\nu \gg 1$ . In this limit, the approximate solution to the above equation is found by balancing the term  $54\nu x [\ln(1/x)]^{7/3}$  against  $18[\ln(1/x)]^2$ . This simplifies the previous equation to  $3\nu x [\ln(1/x)]^{1/3} = 1$ , which we solve iteratively to obtain  $x \approx 1/[3\nu(\ln 3\nu)^{1/3}]$ .

To find the slope of the characteristic and the differential resistivity at depinning, we need to evaluate the quantity  $y = 3\nu x [\ln(1/x)]^{1/3}$  (see Eq. (88)). Rewriting Eq. (D12) gives

$$\begin{aligned} y - \frac{y}{2 \ln(1/x)} + \frac{2}{9} \frac{y}{[\ln(1/x)]^2} - 1 \\ + \frac{1}{\ln(1/x)} + \frac{1}{9[\ln(1/x)]^2} = 0 \end{aligned}$$

Treating the small parameter  $[\ln(1/x)]^{-1} \approx (\ln 3\nu)^{-1}$  perturbatively, we arrive at the solution  $y \approx 1 - (2 \ln 3\nu)^{-1}$ . Substituting further to the expression for differential resistivity gives  $\rho(j_{\text{dp}})/\rho_{\text{ff}} \approx (1/3)[1 - (3 \ln 3\nu)^{-1}]$ .

## Appendix E: Scaling functions

The scaling functions  $g(\kappa)$ ,  $a(\kappa)$ , and  $h(\kappa)$  for marginally strong pinning have been calculated in Appendix A and its asymptotic scaling for very strong pinning has been discussed in Secs. IIIB and IIIC. It remains to determine the function  $\varphi(\kappa)$  defined in Eq. (72); this can be obtained from an expansion of the barriers and energy jumps around the branch crossing point  $x_0$ . With the jumps realized at the points  $x_{\pm}^{\text{jp}} = x_0 + \delta x_{\pm}$ , we use the expansions

$$U_{\text{dp}}(x_+^{\text{jp}}) = U_0 + U'_{\text{dp}}(x_0)\delta x_+, \quad (\text{E1})$$

$$\Delta e_{\text{pin}}(x_+^{\text{jp}}) = -\Delta f_{\text{pin}}(x_0)\delta x_+, \quad (\text{E2})$$

$$U_{\text{p}}(x_-^{\text{jp}}) = U_0 + U'_{\text{p}}(-x_0)\delta x_-, \quad (\text{E3})$$

$$\Delta e_{\text{pin}}(x_-^{\text{jp}}) = -\Delta f_{\text{pin}}(-x_0)\delta x_-, \quad (\text{E4})$$

and the symmetries  $U'_{\text{p}}(-x_0) = -U'_{\text{p}}(x_0)$  and  $\Delta f_{\text{pin}}(-x_0) = -\Delta f_{\text{pin}}(x_0)$ . Setting  $U_{\text{dp}}(x_+^{\text{jp}}) = U_{\text{p}}(x_-^{\text{jp}}) = U$ , we rewrite the total energy jump as

$$\Delta e_{\text{pin}}^{\text{tot}} = \Delta e_{\text{pin}}(x_+^{\text{jp}}) - \Delta e_{\text{pin}}(x_-^{\text{jp}}) \quad (\text{E5})$$

$$= \Delta f_{\text{pin}}(x_0) \left[ \frac{U_0 - U}{U'_{\text{dp}}(x_0)} - \frac{U_0 - U}{U'_{\text{p}}(x_0)} \right]. \quad (\text{E6})$$

The last expression is simplified using  $(U_{\text{p}} - U_{\text{dp}})' = (e_{\text{pin}}^{\text{p}} - e_{\text{pin}}^{\text{f}})' = -\Delta f_{\text{pin}}$ . To leading order, we can assume a constant trapping length  $x_-^{\text{jp}} = -x_0$  and obtain

$$\begin{aligned} \varphi(\kappa) &= \frac{x_0}{x_- \Delta e_c} \frac{\partial \Delta e_{\text{pin}}^{\text{tot}}}{\partial (U_0 - U)/e_p} \\ &= \frac{x_0}{x_- \Delta e_c} \frac{e_p}{|U'_{\text{dp}}(x_0)| |U'_{\text{p}}(x_0)|} \frac{\Delta f_{\text{pin}}(x_0)^2}{(U_0 - U)^2}. \end{aligned} \quad (\text{E7})$$

In the marginally strong pinning regime, we use  $x_- \approx x_0$ ,  $|U'_{\text{dp}}(x_0)| = |f_p[r_p(x)] - f_p(r_m)| = |\Delta f_{\text{pin}}(x_0)|/2$ , and similarly  $U'_p(x_0) = |\Delta f_{\text{pin}}(x_0)|/2$ , and hence

$$\varphi(\kappa) \approx \frac{8e_p\gamma}{9C^2}(\kappa - 1)^{-2}, \quad (\text{E8})$$

where we have made use of Eq. (A12). For very strong pinning  $\kappa \gg 1$ , we use  $x_0 \sim \kappa^{1/2}\xi$ ,  $x_- \sim \kappa^{1/(1+n)}\xi$ ,  $\Delta e_c \sim \kappa e_p$ ,  $|U'_{\text{dp}}(x_0)| = \bar{C}[r_{\text{us}}(x_0) - r_p(x_0)] \sim \bar{C}\xi\kappa^{1/2n}$ ,  $U'_p = \bar{C}[r_f(x_0) - r_{\text{us}}(x_0)] \sim \bar{C}\xi\kappa^{1/2}$ , and  $|\Delta f_{\text{pin}}(x_0)| = \bar{C}[r_f(x_0) - r_p(x_0)] \sim \bar{C}\xi\kappa^{1/2}$ , and therefore  $\varphi(\kappa) \sim \kappa^{-\nu'}$  with the power  $\nu' = (3n + 4)/2(n + 1)(n + 2)$ .

Finally, we plot in Fig. 14 the properly scaled factors  $\varphi(\kappa)(\kappa - 1)^2\kappa^{\nu'-2}$ ,  $g(\kappa)(\kappa - 1)^{4/3}$ ,  $a(\kappa)(\kappa - 1)^{3/2}\kappa^{-(3n+4)/(2n+4)}$ , and  $h(\kappa)(\kappa - 1)^{1/2}\kappa^{-(3n+4)/(4n+4)}$ .

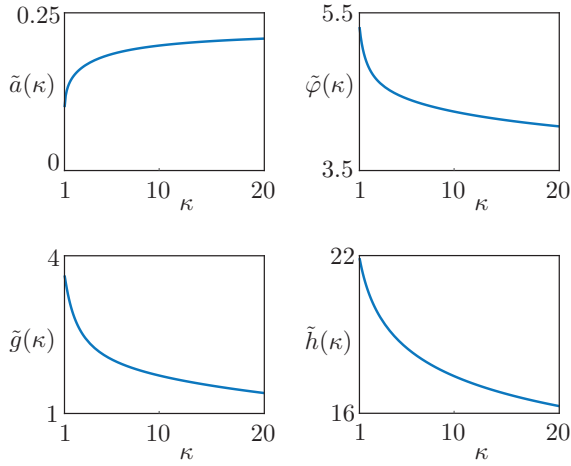


FIG. 14. Rescaled functions characterising the properties of pinning and creep calculated for Lorentzian bare pinning potential. They depend on the pinning strength as described by the Labusch parameter  $\kappa$ . Note the different scales of vertical axes.

## Appendix F: Table of results

- <sup>1</sup> G. Blatter, M. V. Feigel'man, V. B. Geshkenbein, A. I. Larkin, and V. M. Vinokur, *Rev. Mod. Phys.* **66**, 1125 (1994).
- <sup>2</sup> E. H. Brandt, *Reports on Progress in Physics* **58**, 1465 (1995).
- <sup>3</sup> W. Kleemann, *Annual Review of Materials Research* **37**, 415 (2007).
- <sup>4</sup> J. Gorchon, S. Bustingorry, J. Ferré, V. Jeudy, A. B. Kolton, and T. Giamarchi, *Phys. Rev. Lett.* **113**, 027205 (2014).
- <sup>5</sup> M. E. Kassner and M.-T. Pérez-Prado, *Fundamentals of Creep in Metals and Alloys* (Elsevier Science Ltd, Oxford, 2004) pp. 215 – 241.

- <sup>6</sup> C. Zhou, C. Reichhardt, C. J. Olson Reichhardt, and I. J. Beyerlein, *Scientific Reports* **5**, 8000 EP (2015).
- <sup>7</sup> A. I. Larkin and Y. N. Ovchinnikov, *Journal of Low Temperature Physics* **34**, 409 (1979).
- <sup>8</sup> R. Labusch, *Crystal Lattice Defects* **1**, 1 (1969).
- <sup>9</sup> T. Nattermann and S. Scheidl, *Advances in Physics* **49**, 607 (2000), <https://doi.org/10.1080/000187300412257>.
- <sup>10</sup> Y. N. Ovchinnikov and B. I. Ivlev, *Phys. Rev. B* **43**, 8024 (1991).
- <sup>11</sup> A. U. Thomann, V. B. Geshkenbein, and G. Blatter, *Physical Review Letters* **108**, 217001 (2012).
- <sup>12</sup> A. U. Thomann, V. B. Geshkenbein, and G. Blatter, *Phys. Rev. B* **96**, 144516 (2017).

TABLE I. Properties of the pinning energy landscape for a defect with asymptotic decay  $e_p \sim r^{-n}$ ,  $r \gg \xi$ , in the limit of marginally strong and very strong pinning.

Quantity	Exact formula	Marginally strong pinning	Very strong pinning
turning point	$f_p''(r_m) = 0$		
instability points	$f_p'(r_{\pm}) = \bar{C}$	$r_{\pm} - r_m \sim \mp(\kappa - 1)^{1/2}\xi$	$r_- \sim \kappa^{1/(n+2)}\xi$ , $r_+ \sim \xi$
end points	$x_{\pm} = r_{\pm} - \frac{f_p(r_{\pm})}{\bar{C}}$	$x_{\pm} - x_m \sim \pm(\kappa - 1)^{3/2}\xi$	$x_- \sim \kappa^{1/(1+n)}\xi$ , $x_+ \sim \kappa\xi$
critical force density	$F_c = n_p \frac{2x_-}{a_0} \frac{\Delta e_c}{a_0}$	$(\xi/a_0)^2 n_p f_p(\kappa - 1)^2$	$(\xi/a_0)^2 n_p f_p \kappa^{(n+3)/(n+2)}$
frequency factor	$\omega_p(x) = \frac{\sqrt{\lambda_p  \lambda_{us} }}{2\pi\eta a_0^3}$	$\frac{v_p}{\xi}(\kappa - 1)^{1/4} \sqrt{\delta x_+/\xi}$ , $x \rightarrow x_+$ $\frac{v_p}{\xi}(\kappa - 1)$ , $x \approx x_0$	$\frac{v_p}{\xi} \sqrt{\delta x_+/\kappa\xi}$ , $x \rightarrow x_+$ $\left(\frac{x}{\kappa\xi}\right)^{(n+2)/2(n+1)}$ , $x \ll x_+$
frequency factor	$\omega_f(x) = \frac{\sqrt{\lambda_f  \lambda_{us} }}{2\pi\eta a_0^3}$	$\frac{v_p}{\xi}(\kappa - 1)^{1/4} \sqrt{\delta x_-/\xi}$ , $x \rightarrow x_-$ $\frac{v_p}{\xi}(\kappa - 1)$ , $x \approx x_0$	$\frac{v_p}{\kappa^{n/2}\xi} \sqrt{\delta x_+/\kappa\xi}$ , $x \rightarrow x_-$ , $\left(\frac{x}{\kappa\xi}\right)^{(n+2)/2(n+1)} \kappa^{-1/2}$ , $x \gg x_-$
Labusch parameter	$\kappa_{\pm} = \frac{\xi  f_p''(r_{\pm}) }{\bar{C}}$	$\sqrt{\kappa - 1}$	$\kappa_+ \sim \kappa$ , $\kappa_- \sim \kappa^{-1/(n+2)}$
depinning barrier	$U_{dp}(x) = e_{pin}^{us}(x) - e_{pin}^p(x)$	$e_p(\kappa - 1)^2 \left[\frac{\delta x_+}{(\kappa - 1)^{3/2}}\right]^{3/2}$ , $x \rightarrow x_+$ $e_p(\kappa - 1)^2$ , $x = x_0$	$e_p \left(\frac{\delta x_+}{\kappa\xi}\right)^{3/2}$ , $x \rightarrow x_+$ , $e_p[1 - \mathcal{O}(\kappa^{n/2(n+1)})]$ , $x = x_0$
pinning barrier	$U_p(x) = e_{pin}^{us}(x) - e_{pin}^f(x)$	$e_p(\kappa - 1)^2 \left[\frac{\delta x_-}{(\kappa - 1)^{3/2}}\right]^{3/2}$ , $x \rightarrow x_-$ $e_p(\kappa - 1)^2$ , $x = x_0$	$e_p \left(\frac{\delta x_+}{\kappa\xi}\right)^{3/2} \kappa^{(n+3)/2(n+2)}$ , $x \rightarrow x_-$ , $e_p[1 - \mathcal{O}(\kappa^{n/2(n+1)})]$ , $x = x_0$
thermal velocity	$v_{th} = \frac{\omega_p T}{U'_{dp}} \Big _{x_+}$	$\frac{T}{e_p}(\kappa - 1)^{1/4} v_p$	$\frac{T}{e_p} \kappa v_p$
scaling factor	$\varphi(\kappa)$ [Eq. (72)]	$(\kappa - 1)^{-2}$	$\kappa^{-\nu'}$ , $\nu' = \frac{3n+4}{2(n+1)(n+2)}$
scaling factor	$g(\kappa)$ [Eq. (76)]	$\mathcal{O}(1)$	$(\kappa - 1)^{-4/3}$
scaling factor	$a(\kappa) = \frac{\kappa_+}{4\pi} \frac{\xi}{x_-} \frac{e_p}{\Delta e_c}$	$(\kappa - 1)^{-3/2}$	$\kappa^{-1/(n+2)}$
scaling factor	$h(\kappa)$ [Eq. (125)]	$(\kappa - 1)^{-1/2}$	$\kappa^{(n+2)/4(n+1)}$

<sup>13</sup> R. Willa, V. B. Geshkenbein, R. Prozorov, and G. Blatter, Phys. Rev. Lett. **115**, 207001 (2015).

<sup>14</sup> R. Willa, V. B. Geshkenbein, and G. Blatter, Phys. Rev. B **93**, 064515 (2016).

<sup>15</sup> R. Willa, V. B. Geshkenbein, and G. Blatter, Phys. Rev. B **92**, 134501 (2015).

<sup>16</sup> G. Blatter, V. B. Geshkenbein, and J. A. G. Koopmann, Phys. Rev. Lett. **92**, 067009 (2004).

<sup>17</sup> J. Koopmann, V. Geshkenbein, and G. Blatter, Physica C: Superconductivity **404**, 209 (2004), proceedings of the Third European Conference on Vortex Matter in Superconductors at Extreme Scales and Conditions.

<sup>18</sup> A. E. Koshelev and A. B. Kolton, Phys. Rev. B **84**, 104528 (2011).

<sup>19</sup> A. E. Koshelev, I. A. Sadovskyy, C. L. Phillips, and

A. Glatz, Phys. Rev. B **93**, 060508(R) (2016).

<sup>20</sup> R. Willa, A. E. Koshelev, I. A. Sadovskyy, and A. Glatz, Superconductor Science and Technology **31**, 014001 (2018).

<sup>21</sup> S. Brazovskii and A. Larkin, Journal de Physique IV Colloque **9**, Pr10 (1999), to be published in Proceedings of ECRYS-99, J. de Physique, Coll., December 1999.

<sup>22</sup> S. Brazovskii and T. Nattermann, Advances in Physics **53**, 177 (2004).

<sup>23</sup> D. S. Fisher, Phys. Rev. Lett. **50**, 1486 (1983).

<sup>24</sup> D. S. Fisher, Phys. Rev. B **31**, 1396 (1985).

<sup>25</sup> L. V. Shubnikov, V. I. Khotkevich, Y. D. Shepelev, and Y. N. Riabinin, [Zh. Eksp. Teor. Fiz. **7**, 221 (1937)] Ukrainian Journal of Physics **53**, 42 (2008).

<sup>26</sup> A. A. Abrikosov, [Zh. Eksp. Teor. Fiz. **32**, 1442 (1957)]



- JETP **5**, 1174 (1957).
- <sup>27</sup> M. Tinkham, *Introduction to Superconductivity* (McGraw Hill, New York, 1996).
  - <sup>28</sup> A. I. Larkin and Y. N. Ovchinnikov, [Zh. Eksp. Teor. Fiz. **65**, 1704 (1974)] JETP **38**, 854 (1974).
  - <sup>29</sup> A. Schmid and W. Hauger, Journal of Low Temperature Physics **11**, 667 (1973).
  - <sup>30</sup> O. Narayan and D. S. Fisher, Phys. Rev. B **46**, 11520 (1992).
  - <sup>31</sup> P. Chauve, T. Giamarchi, and P. Le Doussal, Phys. Rev. B **62**, 6241 (2000).
  - <sup>32</sup> H. Kramers, Physica **7**, 284 (1940).
  - <sup>33</sup> M. Buchacek, R. Willa, V. B. Geshkenbein, and G. Blatter, Phys. Rev. B **98**, 094510 (2018).
  - <sup>34</sup> P. H. Kes, J. Aarts, J. van den Berg, C. J. van der Beek, and J. A. Mydosh, Superconductor Science and Technology **1**, 242 (1989).
  - <sup>35</sup> R. Willa, A. E. Koshelev, I. A. Sadovskyy, and A. Glatz, Phys. Rev. B **98**, 054517 (2018).
  - <sup>36</sup> M. P. Maley, J. O. Willis, H. Lessure, and M. E. McHenry, Phys. Rev. B **42**, 2639 (1990).
  - <sup>37</sup> Y. Yeshurun, A. P. Malozemoff, and A. Shaulov, Rev. Mod. Phys. **68**, 911 (1996).
  - <sup>38</sup> S. Eley, M. Miura, B. Maiorov, and L. Civale, Nature Materials **16**, 409 EP (2017).
  - <sup>39</sup> P. W. Anderson, Phys. Rev. Lett. **9**, 309 (1962).
  - <sup>40</sup> G. Blatter, V. B. Geshkenbein, and V. M. Vinokur, Phys. Rev. Lett. **66**, 3297 (1991).
  - <sup>41</sup> Z. L. Xiao, E. Y. Andrei, Y. Paltiel, E. Zeldov, P. Shuk, and M. Greenblatt, Phys. Rev. B **65**, 094511 (2002).
  - <sup>42</sup> Z. L. Xiao, E. Y. Andrei, Y. Paltiel, E. Zeldov, P. Shuk, and M. Greenblatt, private communication.
  - <sup>43</sup> I. Roy, S. Dutta, A. N. Roy Choudhury, S. Basistha, I. Maccari, S. Mandal, J. Jesudasan, V. Bagwe, C. Castellani, L. Benfatto, and P. Raychaudhuri, Phys. Rev. Lett. **122**, 047001 (2019).
  - <sup>44</sup> I. Roy, S. Dutta, A. N. Roy Choudhury, S. Basistha, I. Maccari, S. Mandal, J. Jesudasan, V. Bagwe, C. Castellani, L. Benfatto, and P. Raychaudhuri, private communication.
  - <sup>45</sup> M. Buchacek, V. B. Geshkenbein, and G. Blatter, unpublished.
  - <sup>46</sup> Y. Iye, T. Tamegai, H. Takeya, and H. Takei, Japanese Journal of Applied Physics **26**, L1057 (1987).
  - <sup>47</sup> T. T. M. Palstra, B. Batlogg, L. F. Schneemeyer, and J. V. Waszczak, Phys. Rev. Lett. **61**, 1662 (1988).
  - <sup>48</sup> M. Tinkham, Phys. Rev. Lett. **61**, 1658 (1988).
  - <sup>49</sup> A. Larkin, [ZhETF, **58** (4), 1466 (1970)] JETP **31**, 784 (1970).